https://doi.org/10.1016/j.epsl.2024.118982

Interplay and feedback between tectonic regime, faulting, sealing horizons, and fluid flow in a hydrocarbon-hosting extensional basin: the Val d'Agri Basin case, southern Italy

Schirripa Spagnolo G.[1], Bernasconi S.M.[2], Aldega L.[1], Castorina F.[1,3], Billi A.[3], Smeraglia L.[3], Agosta F.[4], Prosser G.[4], Tavani S.[3,5], Carminati E.[1]

1 – Dipartimento di Scienze della Terra, Sapienza Università di Roma, Rome, Italy

2 - Department of Earth Sciences, ETH Zurich, Zurich, Switzerland

3 – Consiglio Nazionale delle Ricerche, IGAG, Rome, Italy

4 - Dipartimento di Scienze, Università della Basilicata, Potenza, Italy

5- DISTAR, Università degli Studi di Napoli Federico II, Napoli, Italy

Keywords:

extensional basin; hydrocarbon reservoir; seal integrity; carbonate clumped isotopes; active faulting; fluid circulation systems.

Abstract

Understanding the factors that govern past fluid circulation in tectonically active and/or hydrocarbon-rich basins is crucial for elucidating present-day fluid-flow scenarios. We investigate the circulation of paleo-fluids in the extensional-transtensional Val d'Agri Basin (southern Italy), home to a giant oil field and significantly affected by both natural and human-induced seismicity. Our aim is to understand how faulting and the variable thickness of the clay-rich tectonic mélange, which constitutes the seal of the hydrocarbon reservoir, influenced past fluid flow under different tectonic regimes. To achieve this, we combined multiscale structural observations with isotope (C, O, clumped, and Sr) and Rare Earth and Yttrium (REY) analyses of fault-related calcite mineralizations. Using analytical methodologies that allow the analysis of sub-milligram samples for carbonate clumped isotopes, we provided a detailed characterization of the variability in precipitation temperatures and composition of parental fluids in both space and time. Our results reveal five main types of parental fluids, ranging from meteoric to intraformational and deep crustal, which were differently involved in the tectonic evolution of the Val d'Agri Basin. During orogenic shortening, vertical fluid circulation was mostly limited and compartmentalized, whereas post-orogenic extensional faulting promoted the ascent of deep fluids. Our findings indicate that the sealing properties of the mélange were likely enhanced locally by increased thickness but were also compromised by fault activity and associated seismic events. Fluid circulation in the study area has been influenced by the prevailing tectonic regime (compressive vs. extensional), stratigraphic-structural architecture, properties of impermeable horizons, and seismic events. The model proposed for the Val d'Agri Basin elucidates past processes that are useful for understanding current fluid circulation in the basin itself and can be applied to other basins where fluid circulation is partly manipulated by human activities.

1. Introduction

In various tectonic settings (e.g., extensional basins, fold-and-thrust belts, etc.), accumulation of fluids in the subsurface, including groundwater, hydrocarbons, and CO_2 is ruled by stratigraphical, lithological and mechanical properties of the sealing horizons (Grunau, 1987). These impermeable horizons, which are often clay-rich, maintain fluid confinement potentially causing fluid overpressures (Hager et al., 2021). The sealing capacity of impermeable horizons can be compromised by fault zones, which can act as fluid conduits (Caine et al., 1996; Faulkner et al., 2010) or cause fault-valve actions (Sibson, 2000; Doglioni et al., 2014). In tectonically active regions, changes in pore fluid pressure and its diffusion can trigger both natural (Miller et al., 2004) and human-induced (Ellsworth, 2013) earthquakes. Consequently, understanding the complex interaction between fluids, faults, and impermeable horizons is of significant economic and social importance, particularly for fluid exploitation (Song et al., 2022), storage (Shukla et al., 2010), and assessment of seismic and environmental hazards (Chiodini et al., 2020).

The Val d'Agri Basin in southern Italy serves as an outstanding natural laboratory for investigating the above-mentioned geological processes. It is a seismically active intermontane basin formed since the Middle-Late Pleistocene due to post-orogenic extensional-transtensional faulting, which dissected and partly reactivated pre-existing tectonic structures (Patacca & Scandone, 2007). The structural architecture of this basin, resulting from its polyphasic tectonic history, led to the genesis of the largest onshore oil field in western Europe. Hydrocarbons are trapped below a clay-rich, fluid-overpressured, and impermeable sealing horizon, known as the Irpinia mélange (Mazzoli et al., 2001; Hager et al., 2021). Both lateral distribution and vertical integrity of the Irpinia mélange are subjects of an extensive debate (Brozzetti, 2011; Candela et al., 2015; D'Adda et al., 2017). Additionally, the Val d'Agri Basin has experienced historical strong earthquakes (M≤7; Cucci et al., 2004) and recent low-magnitude seismicity (M≤3; Improta et al., 2017) of both natural and induced origins.

In this study, we elucidate the interplay and feedback between fluid flow, faulting, and the Irpinia mélange. We focus on the evolution of paleo-fluid circulation both in space and time to deepen our understanding of current fluid circulation and envision future scenarios. We carry out a structural-geochemical study of syn-tectonic calcite mineralizations collected within fault zones of the Val d'Agri Basin to reconstruct a basin-scale, spatiotemporal conceptual model of fluid flow. Through geochemical analyses, including the largest database of carbonate clumped isotopes applied to a single case study so far, we reveal significant variability in fault-fluid interaction processes. These insights are valuable for evaluating the current integrity of sealing horizon in the Val d'Agri area, and in other hydrocarbon-rich post-orogenic extensional basins worldwide (e.g., Pannonian Basin, Hungary, Czauer & Madl-Szonyi, 2011; Bohai Bay Basin, China, Song et al., 2022; Nispiro Field, Mexico, Bourdet et al., 2010).

2. Geological Setting

The Val d'Agri is a post-orogenic extensional-transtensional basin located in the Southern Apennines fold-and-thrust belt, Italy. The Southern Apennines ensued from the superimposition of orogenic and post-orogenic tectonic phases, which were associated with the eastward retreat of the westward-subducting Adriatic slab, and with the opening of the Tyrrhenian back-arc basin (e.g., Malinverno and Ryan, 1986). The orogenic shortening resulted in the stacking of tectonic units derived from the Mesozoic oceanic (Ligurian Accretionary Complex) and Adriatic passive margin domains (i.e., Apennine and Apulian Carbonate Platforms, Lagonegro Basin; Patacca and Scandone, 2007; Fig. 1), which were differentiated during Mesozoic rift-related extensional tectonics and subsequent oceanization (Patacca and Scandone, 2007). Since the Miocene time, these units were detached from their original substratum, and overthrusted toward the foreland with a ca. NE-directed motion. The final orogenic phase (Late Pliocene-Early Pleistocene) was associated with a shift from thin- to thick-skinned tectonics (Shiner et al., 2004; Butler et al., 2004). Middle Pleistocene-Holocene, post-orogenic, extensional-transtensional tectonics led to the displacement or reactivation of pre-existing structures and gave rise to numerous intermontane basins including the Val d'Agri Basin (Patacca and Scandone, 2007). Within the Val d'Agri basin area, the superimposition of distinct thrust sheets, characterized by varying lithology, thickness, rheology, and permeability (Fig. 1; Patacca and Scandone, 2007) determined the genesis of the largest onshore oil field in western Europe. Its tectono-stratigraphic succession includes, from top to bottom: siliciclastic-carbonate turbidites (Albidona and Gorgoglione fms.), shallow-marine carbonates of the Apennine Platform, proximal-to-distal pelagic successions of the Lagonegro Basin, the Irpinia mélange, and shallow-marine carbonates of the Apulian Platform (Shiner et al., 2004; Patacca & Scandone, 2007; Palladino et al., 2023; Fig. 1b). The Irpinia mélange, a heterogeneous, tectonic, clay-rich, 0.1 to~ 1 km thick (Mazzoli et al., 2001) horizon with a general permeability of < 10^{-7} mD (Hager et al., 2021), forms the seal of the Val d'Agri hydrocarbon reservoir constituted by the Apulian Carbonate Platform.

The basin is bordered by two main fault systems: the East Agri Fault System (EAFS; Fig. 1d), to the northeast, and the Monti della Maddalena Fault System (MMFS; Fig.1d), to the southwest. Both fault systems are primarily composed of steeply dipping, NW-SE and NE-SW striking, extensional-transtensional faults (e.g., Giano et al., 2000; Schirripa Spagnolo et al., 2024). These structures are consistent with the present NE-SW oriented tectonic extension (Mariucci and Montone, 2020). The two fault systems are secondarily composed of faults with a wide range of orientations. While some authors consider all these faults as the result of the polyphase tectonic history (e.g., Cello et al., 2000), a recent model proposes a polygonal-like style of faulting controlled by the Irpinia mélange (Schirripa Spagnolo et al., 2024). However, the role of this mélange during post-orogenic extension is not well understood. Some studies contend that the Val d'Agri faults root along the Irpinia mélange, decoupling the Apulian Carbonate Platform from the overlying units (D'Adda et al., 2017; Hager et al., 2021). This resulted in the soft-linkage between shallow extensional faults and deep inherited structures within the Apulian Carbonate Platform (Borraccini et al., 2002; Candela et al., 2015). Conversely, others suggest that the main faults of both EAFS and MMFS cut across and displace the Irpinia mélange (Brozzetti, 2011; Valoroso et al., 2023).

Schirripa Spagnolo et al. (2024) performed the first radiometric dating of the Val d'Agri fault activity, yielding two reliable U–Pb ages. In particular, they dated slip along two extensional faults. One slickenfiber was dated at 0.82±1.28 Ma, and hence interpreted as due to the Pleistocene-Holocene extensional phase. The other slickenfiber yielded a 13.5±2.47 Ma age, and interpreted as pre-thrusting, foreland flexure-related, Early-Middle Miocene extensional stage. However, this slickenfiber is crosscut by a second generation of slickenfibers with normal movement, indicating that the fault was later reactivated. The Quaternary seismic activity of the Val d'Agri fault systems is constrained by paleoseismological, historical, and instrumental data (e.g., Giano et al., 2000; Improta et al., 2017). The most destructive historical earthquakes occurred in 1857 (Mw = 7.1) with an uncertain source, which is either postulated to be the EAFS (Benedetti et al., 1988; Bello et al., 2022) or the MMFS (Maschio et al., 2005; Improta et al., 2010). Recent background seismicity is either of natural and/or man-made origin. Natural seismicity is consistent with the present NE-SW oriented extension (Maggi et al., 2009; Improta et al., 2017) and is primarily correlated with the southernmost segments of the MMFS (Valoroso et al., 2009; Improta et al., 2017). Induced events were triggered by oscillations in the water level of Pertusillo lake (Fig. 1c) or by wastewater re-injection during hydrocarbon extraction (Improta et al., 2017; Valoroso et al., 2023). The interaction between fluids and seismic activity in the study area is further evidenced by hydrogeochemical anomalies detected in a 400 m deep exploration well in the MMFS (i.e., Tramutola oil seep; Fig. 1d), which revealed significant short-term geochemical variations before and after two moderate earthquakes in 1996 (M_L = 4.9; Italiano et al., 2001) and 2004 (M_L = 4.1; Colangelo et al., 2007). Since the 1860 earthquake, natural hydrocarbon emissions have been documented in the area surrounding this well (Colangelo et al., 2005).

Previous studies have examined syn-tectonic mineralizations exposed near Marsico Nuovo (Fig. 1c). They revealed the involvement of diagenetic fluids during the early orogenic shortening stage (Miocene; Iannace et al., 2012; Gabellone et al., 2013), of deep dolomitizing fluids likely originated from the Irpinina mélange during the late orogenic shortening stage (Pliocene; Iannace et al., 2012; Gabellone et al., 2013), and of warm fluids (130°-140°) during the post-orogenic extension (Pleistocene-Holocene; Mazzoli et al., 2004).

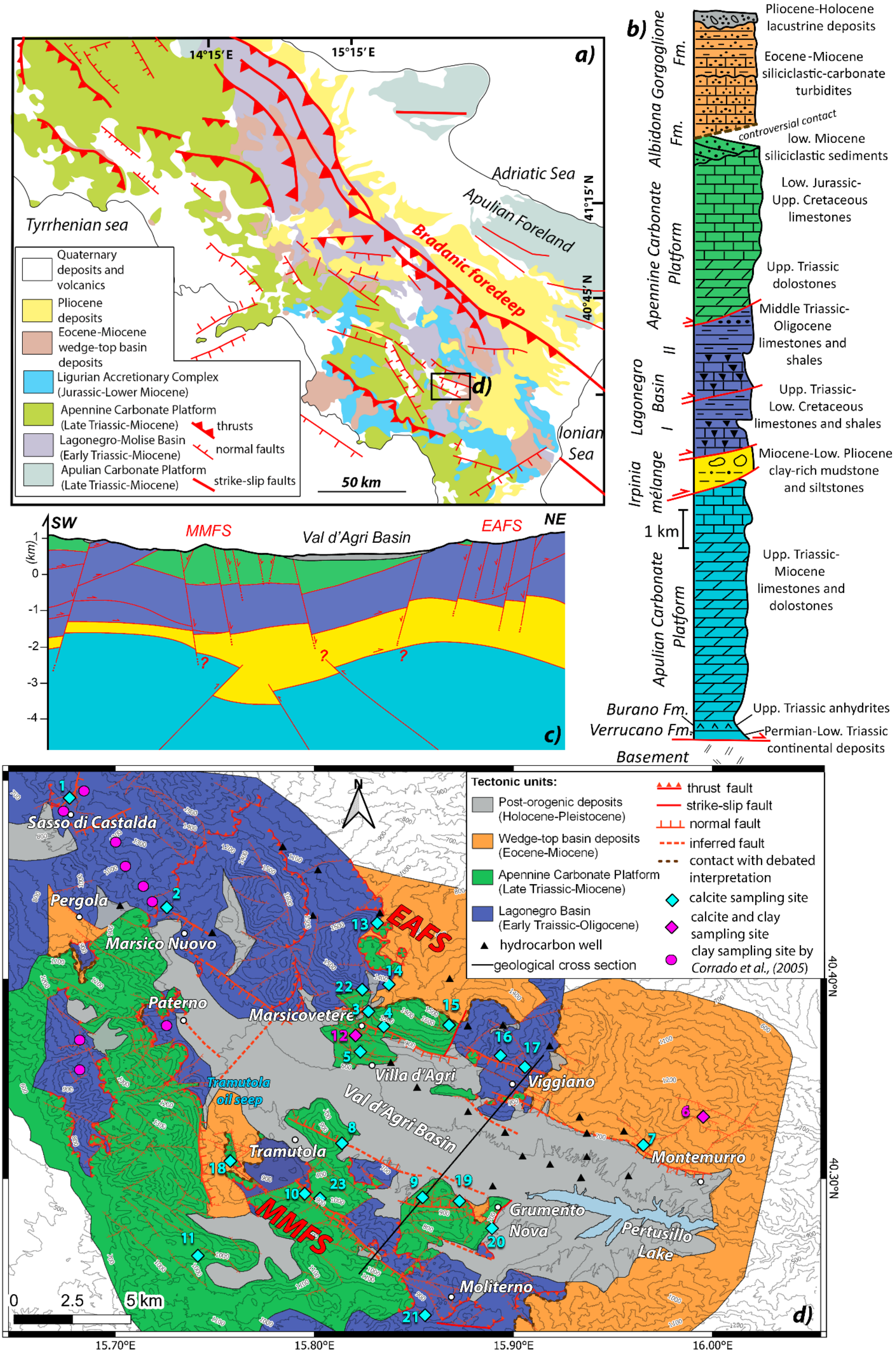
a)
14°15′E
15°15′E
41°15′N
40°45′N
Adriatic Sea
Apulian Foreland
Bradanic foredeep
Tyrrhenian sea
Ionian Sea
d)
Quaternary deposits and volcanics
Pliocene deposits
Eocene-Miocene wedge-top basin deposits
Ligurian Accretionary Complex (Jurassic-Lower Miocene)
Apennine Carbonate Platform (Late Triassic-Miocene)
Lagonegro-Molise Basin (Early Triassic-Miocene)
Apulian Carbonate Platform (Late Triassic-Miocene)
thrusts
normal faults
strike-slip faults
50 km
b)
Albidona Fm.
Gorgoglione Fm.
Pliocene-Holocene lacustrine deposits
Eocene-Miocene siliciclastic-carbonate turbidites
controversial contact
low. Miocene siliciclastic sediments
Apennine Carbonate Platform
Low. Jurassic-Upp. Cretaceous limestones
Upp. Triassic dolostones
Lagonegro Basin
II
I
Middle Triassic-Oligocene limestones and shales
Upp. Triassic-Low. Cretaceous limestones and shales
Irpinia mélange
Miocene-Low. Pliocene clay-rich mudstone and siltstones
1 km
Apulian Carbonate Platform
Upp. Triassic-Miocene limestones and dolostones
Burano Fm.
Upp. Triassic anhydrites
Verrucano Fm.
Permian-Low. Triassic continental deposits
Basement
c)
SW
NE
MMFS
Val d'Agri Basin
EAFS
(km)
1
0
-1
-2
-3
-4
?
d)
Tectonic units:
Post-orogenic deposits (Holocene-Pleistocene)
Wedge-top basin deposits (Eocene-Miocene)
Apennine Carbonate Platform (Late Triassic-Miocene)
Lagonegro Basin (Early Traissic-Oligocene)
hydrocarbon well
geological cross section
thrust fault
strike-slip fault
normal fault
inferred fault
contact with debated interpretation
calcite sampling site
calcite and clay sampling site
clay sampling site by Corrado et al., (2005)
N
Sasso di Castalda
Pergola
Marsico Nuovo
Paterno
Marsicovetere
Villa d'Agri
Viggiano
Tramutola oil seep
Val d'Agri Basin
Tramutola
Montemurro
Grumento Nova
Pertusillo Lake
Moliterno
EAFS
MMFS
1
2
3
4
5
6
7
8
9
10
11
12
13
14
15
16
17
18
19
20
21
22
23
0
2.5
5 km
40.40°N
40.30°N
15.70°E
15.80°E
15.90°E
16.00°E

Fig. 1. a) Structural-tectonic map of the Southern Apennines modified by Maggi et al. (2009) and Vitale & Ciarcia (2018), showing the location of panel-d. b) Tectono-stratigraphy succession with lithological description of tectonic units (Butler et al., 2004; Mazzoli et al., 2001; Patacca & Scandone, 2007; Palladino et al., 2023); c) Schematic cross-section (modified after Schirripa Spagnolo et al., 2024), whose trace is reported in panel-d; d) Structural-tectonic map of the Val d'Agri Basin (modified after Beaubien et al., 2023), showing sampling sites (blue-sky diamonds). EAFS: East Agri Fault System; MMFS: Monti della Maddalena Fault System.

3. Methods

We collected 351 fault-related calcite mineralizations from fault zones pertaining either to the EAFS or to the MMFS, as well as 33 host rock samples representative of different tectonic units (Fig. 1c; Tables S1-S2). Far from the EAFS and MMFS fault zones, background veins with thickness suitable for micro-drilling are very rare, and generally oriented parallel to the bedding. Therefore, these veins are not statistically significant and were not sampled. Based on the amount of available material, we selected samples for the following analyses: 1) measurements of vein attitudes and of fault attitudes and kinematics; 2) microstructural observations of 42 thin sections by optical and cathodoluminescence microscopy; 3) carbon and oxygen isotope of 351 fault-related calcite mineralizations and 33 calcite host rocks using a Thermofisher GasBench, requiring 100-150 μg of sample; 4) carbonate clumped isotopes of 75 fault-related calcite mineralizations, using a Thermo Scientific Kiel IV-MAT253 system, which provides accurate results with only 400-800 μg of sample (Muller et al., 2017). From clumped measurements ($\Delta_{47;}$ I-CDES) we derive precipitation temperatures ($T\Delta_{47;}$ °C) and oxygen isotope compositions of parental fluids using calibrations of Anderson et al. (2021) and O'Neil et al. (1969), respectively ; 5) rare earth elements and yttrium (REY) of 9 fault-related calcite mineralizations and 3 host rock samples using a ICP mass spectrometer, requiring 5g of sample; 6) $^{87}Sr/^{86}Sr$ ratio of 12 selected fault-related calcite mineralizations using a FINNIGAN MAT mass spectrometer requiring 20 mg of sample; 7) mineralogy of two clay-rich interbedded layers using a X-ray system equipped with silicon-strip detector, requiring 15g of sample. Detailed descriptions of the analytical methods are provided in the Supplementary Materials.

4. Results

4.1. Meso-structural Observations

Among the 351 fault-related calcite mineralizations, we distinguish between those that are clear kinematic indicators and those that are not. In the Discussions section, we assign all mineralizations to the compressional or extensional tectonic phase with different degrees of confidence (Roberts & Holdsworth, 2022). Mineralizations that are fault kinematic indicators are classified using the terminology of Van Der Pluijm & Marshak (2004) and include:

- slickenfibers on fault surfaces characterized by mineral growth lineations primarily indicating extensional shear sense, with a few exceptions showing compressional kinematics (Fig. 2a; Table S1).
- pinnate veins immediately adjacent to fault surfaces, forming an acute angle of 30°-45° relative to the fault plane and indicating extensional shear (Fig. 2b; Table S1).
- tension gashes characterized by sigmoidal shape along tension fractures, displaying contractional, strike-slip (both dextral and sinistral), or extensional shear (Fig. 2c; Table S1).

Other mineralizations, not associated with kinematic indicators, display a wide range of orientations (Fig. 2a), and are classified using geometric criteria. They include:

- gently dipping veins, with dip angles between 5° and 45° (Fig. 2a). Generally parallel to bedding or cleavage (Table S2), these veins are, in some cases, crosscut by extensional-transtensional faults (Fig. 2d).
- steeply dipping veins, with dip angles between 50° and 90° (Fig. 2a, e). When bedding is recognizable, cut-off angles between vein and bed are > 50° (Table S2).
- stockwork veins, characterized by nonsystematic orientation, irregular shapes, and nonplanar array. These veins occur within pervasively fractured rocks, primarily at the footwall of the extensional-transtensional faults (Fig. 2f).
- banded veins, without any preferential attitude, and composed of 3 to 10 cm-wide white to brownish bands (Tables S1-2; Fig. 2g). These veins cut across bedding as well as extensional-transtensional faults and fractures (Fig. S1).

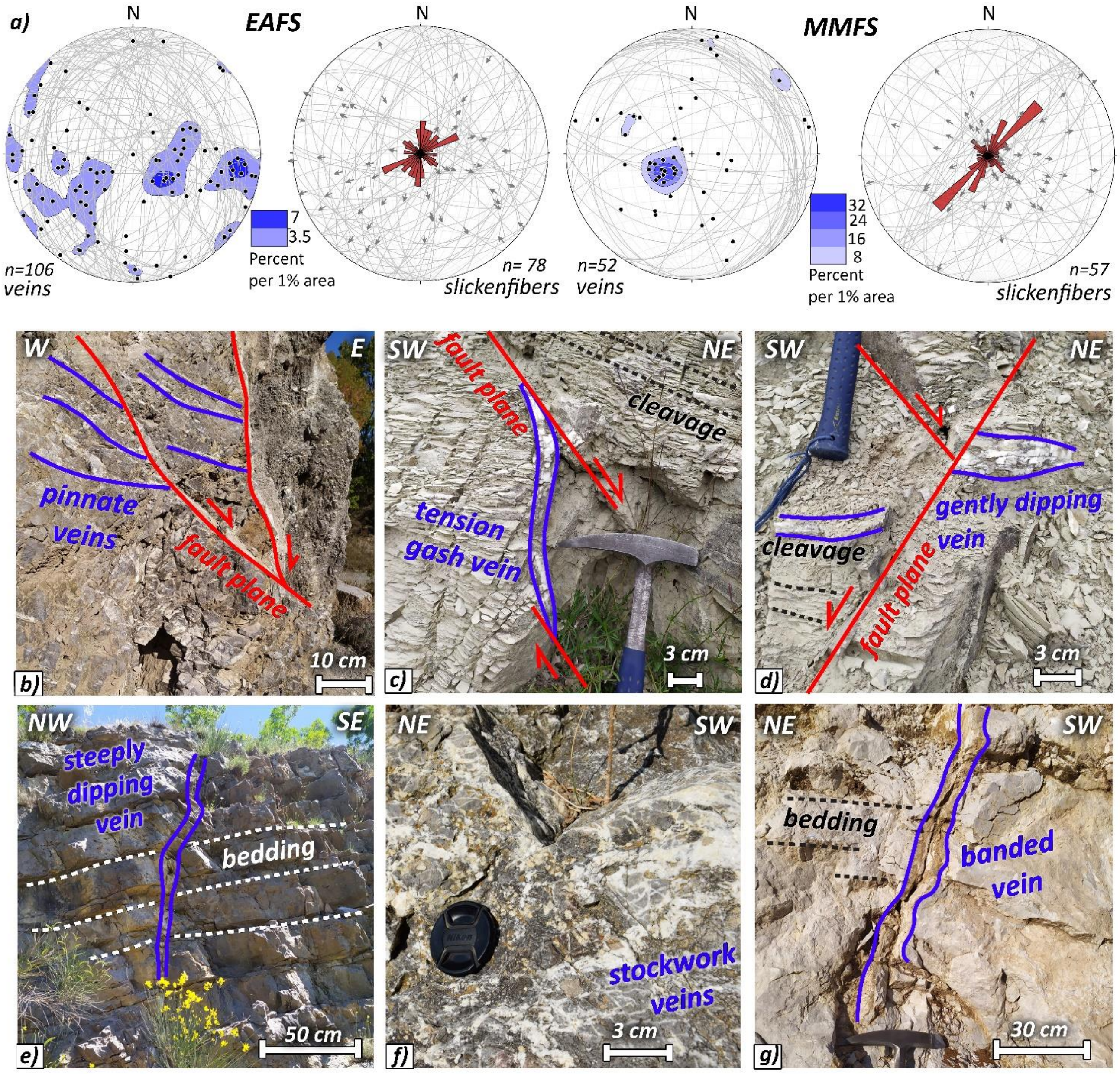

Fig. 2. *a) Schmidt projections (lower hemisphere) distinguished on EAFS and MMFS provenance, showing attitudes of veins and fault planes with striae (grey), pole contour of veins (blue), and rose diagram of faults decorated by slickenfibers (red). b) Outcrop picture (sampling site 10; Fig. 1) of pinnate veins, associated with extensional faults; c) Outcrop picture (sampling site 6; Fig. 1) of sigmoidal tension gash vein, associated with extensional shear; d) Outcrop picture (sampling site 7; Fig. 1) of gently dipping vein, almost parallel to cleavage and cut by an extensional fault; e) Outcrop picture (sampling site 2; Fig. 1) of steeply dipping vein, with cut-off angles between vein and bed of ~70°; f) Outcrop picture (sampling site 1; Fig. 1) of stockwork veins sampled at the footwall of a regional transtensional fault; g) Outcrop picture (sampling site 5; Fig. 1) of banded vein.*

4.2. Microstructures

- Slickenfibers are characterized by blocky crystals and are frequently associated with coat breccias and cataclastic fault-rocks rich in veins (Fig. 3a). MAR29 and MAR8 samples exhibit crosscutting relationships, indicating two growth events (Fig. S2).
- Steeply to gently dipping and stockworks veins are composed of blocky calcite crystals with thin to thick twinning (Fig. 3). GIU22 and MA25 stockwork vein samples also show fibrous crystals (Figs. 3c, d). In some steeply and gently dipping veins (samples VA24, VA25, MA46, S10-39; Figs. 4 and S5), different crystal growth phases are identified. Furthermore, in samples including stylolites (Figs. 3d-f, S6), veins cut across them (sample VA17) or exhibit mutually crosscutting relationships (samples VA25, MA20, MA25, GIU22, and GIU33).
- Banded veins are characterized by blocky-elongated calcite crystals, with crystal growth competition, thin twinning, and inclusion bands parallel to vein walls (Fig. 3). Less commonly, alabastrine-like textures and open vugs are also present. Samples S2G1, S2G8, and S2G18 exhibit fractured crystals, indicating multiple growth phases (Fig. S1).

The cathodoluminescence colors of these syn-kinematic calcite mineralizations are lithology-dependent (Fig. 4). Slickenfibers and veins in the Lagonegro Basin (Figs. 4e, f, S5) and Albidona Fm. (Figs. 4c, d, S4) show bright red luminescence, which is duller, homogeneous, or brighter than that of the host rock (except for sample MA52, which is completely not luminescent; Fig. S2). Conversely, syn-kinematic calcite mineralizations within the Apennine Carbonate Platform are non-luminescent (Figs. S1-2) or show dull red luminescence similar to that of the host rock (Figs. 4a, b, S3).

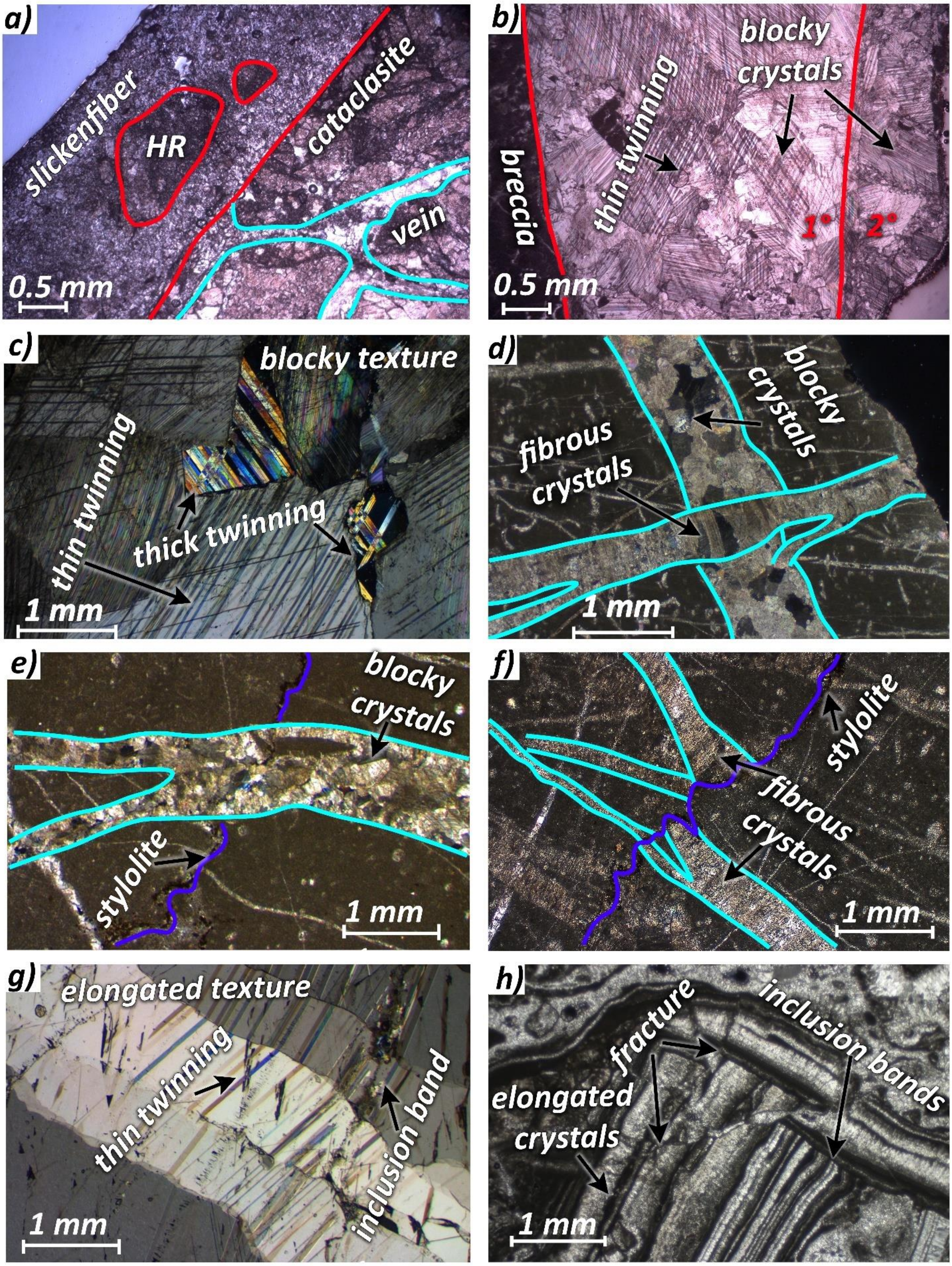
a)
slickenfiber
HR
cataclasite
vein
0.5 mm
b)
breccia
thin twinning
blocky crystals
1°
2°
0.5 mm
c)
blocky texture
thin twinning
thick twinning
1 mm
d)
blocky crystals
fibrous crystals
1 mm
e)
blocky crystals
stylolite
1 mm
f)
stylolite
fibrous crystals
1 mm
g)
elongated texture
thin twinning
inclusion band
1 mm
h)
fracture
inclusion bands
elongated crystals
1 mm

219

220

Fig. 3 Optical images of: a) slickenfiber (MAR31 sample; Table S1), which coat cataclasite with veins; b) slickenfibers (MAR8 sample; Table S1) formed by two generations of blocky calcite crystals (1°, the oldest, and 2°, the youngest); c) blocky texture with thin and thick twinning (S9-22 sample; Table S1); d) a vein with fibrous crystals which cut through a vein with blocky crystals (MA25 sample; Table S1); e) a vein with blocky crystals which cut through a stylolite (VA17 sample; Table S1); f) veins with fibrous crystals cut by stylolites (GIU22 sample; Table S1); g) vein with elongated texture, thin twinning and inclusion bands (VA39 sample, Table S1); h) vein with fractured elongated crystals (S2G8 sample; Table S1). All images are taken with cross-polarized light except for panel a, for which plane-polarized light was used.

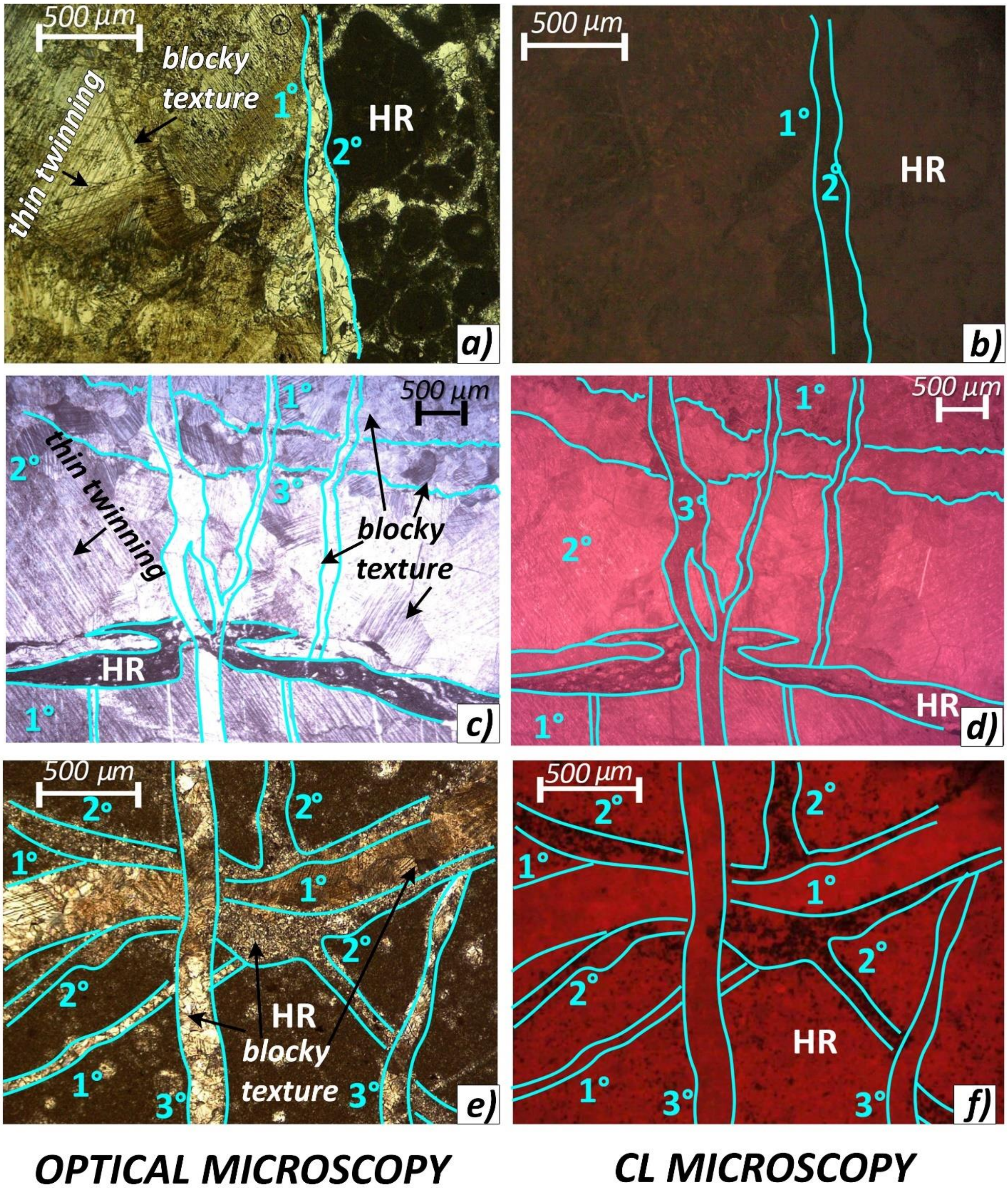

Fig. 4 a), b) Optical and cathodoluminescence (CL) microscopy images of veins from the Apennine Carbonate Platform (MA46 sample; Table S1), which show dull luminescence. c), d) Optical and CL microscopy images of veins from the Albidona Fm., (S10-39 sample; Table S1), which show intense luminescence. e), f) Optical and CL microscopy images of veins from the Lagonegro Basin unit (VA25 sample; Table S1), which show intense luminescence. HR: host rocks. Sky blue numbers refer to different generations of calcite crystals, from the oldest (1) to the youngest (3). All optical images are taken using plane-polarized light.

4.3. Clay mineralogy

We carried out XRD analyses to further constrain the 1D burial and thermal models by Aldega et al. (2003) and Corrado et al. (2005) that indicate a maximum burial temperature of 140°-160°C for the Triassic-Jurassic limestones of the Lagonegro Basin due to a tectonic loading of 4-4.5 km. We analyzed two clay-rich layers interbedded within the Albidona Fm. (MAR42, Table S1; at site 6, Fig. 1c), and the Cretaceous limestones of the Apennine Carbonate Platform (MAR11, Table S1; at site 12, Fig. 1c) both overlying the Lagonegro Basin unit. The sample from the Albidona Fm. consists of kaolinite (61%), subordinate amounts of mixed layer illite-smectite (I-S, 20%), illite (18%), chlorite (1%), and traces of calcite and goethite (<1%). Mixed layers I-S mainly correspond to short-ordered structures (R1) with an illite content of 73% (Fig. S7), indicating the first stages of deep diagenesis with an approximate maximum temperature of 110°-120°C (e.g., Środoń, 1999). The XRD pattern also shows a small hump at 5.2°2θ and aperiodic *00l* diffraction peaks interpreted as random ordered mixed layer I-S (R0).

The sample from the Cretaceous limestone of the Apennine Platform contains kaolinite (35%), illite (36%), two populations of mixed layers illite-smectite (26%), and low chlorite contents (3%). The most abundant population of I-S corresponds to short-ordered structures (R1) with an illite content of 78% (Fig. S7), whereas the second is composed of random ordered I-S (R0). This assemblage indicates a temperature range of 100°-110°C (Środoń, 1999).

Temperatures of 100°-120°C obtained for the Apennine Carbonate Platform and Albidona Fm. overlying the Lagonegro Basin unit are consistent with Aldega et al. (2003) and Corrado et al. (2005) who determined that the Miocene deposits at top of the Lagonegro succession (Fig. 1b) experienced maximum burial temperatures of 110°-120°C. Results from MAR11 and MAR 42 as well as from the Lagonegro succession (Aldega et al., 2003; Corrado et al., 2005) document that I-S formed during diagenetic overprint as a result of Miocene tectonic burial (Fig. S8).

4.4. Carbon, Oxygen, and Carbonate Clumped Isotopes

The carbon and oxygen isotope compositions of veins and slickenfibers, along with those of the corresponding host rocks, are presented in Figure 5. The data from the Apennine Carbonate Platform are divided into two plots, separating samples from the EAFS and MMFS (Figs. 5c, d). The Apennine Carbonate Platform is extensively exposed along both the EAFS and the MMFS, whereas the Albidona Fm. and Lagonegro Basin rocks are predominantly exposed along the EAFS. Therefore, Figures 5a and 5b exclusively present data from the EAFS, with three exceptions indicated by circles in Figure 5a.

The Lagonegro Basin rocks are characterized by a $\delta^{18}O$ values between +26.3 and +26.7‰ V-SMOW and by $\delta^{13}C$ values between +2.1 and + 2.3‰ V-PDB (Fig. 5a). The Albidona Fm. rocks show $\delta^{18}O$ values between +26.9 and +27.9‰, and $\delta^{13}C$ values between +0.5 and +0.9‰ (Fig. 5b). The Apennine Carbonate Platform rocks exhibit by $\delta^{18}O$ values between +28.3 and +29.9‰, and $\delta^{13}C$ values between +1.3 and +2.2‰ along the EAFS (Fig. 5c), and by $\delta^{18}O$ values between +27.9 and +29.7‰, and $\delta^{13}C$ values between +0.5 and +1.5‰ along the MMFS (Fig. 5d). In Figure 5 we categorize veins and slickenfibers based on their $\delta^{13}C$. Samples with negative $\delta^{13}C$ define cluster 1. Among the samples with positive $\delta^{13}C$, we define cluster 2 for veins and slickenfibers that have a $\delta^{18}O$ more than 5‰ lower than the host rocks. Cluster 3 includes veins and slickenfibers with $\delta^{18}O$ within 5‰ of the host rocks.

The Lagonegro Basin and the Albidona Fm. mineralizations show a relatively small variability and mostly belong to cluster 3 (Figs. 5a and b). The Apennine Carbonate Platform mineralizations show more scattered $\delta^{18}O$ values, falling into all three calcite clusters. Clusters 2 and 3 are well defined in samples from the EAFS (Fig. 5c), whereas they are not clearly separated in samples from the MMFS (Fig. 5d).

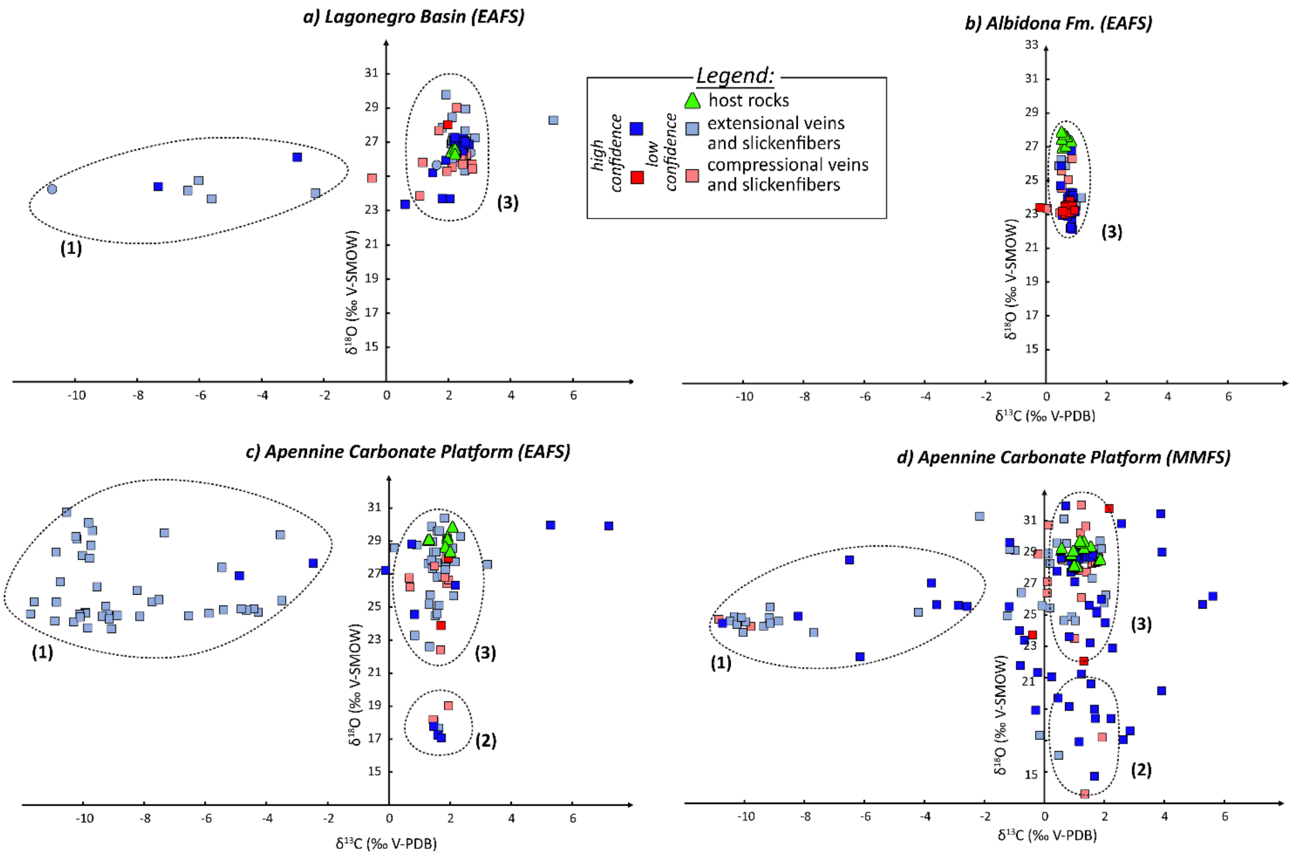

<u>Fig. 5.</u> δ ^{13}C vs. δ ^{18}O plots of calcite mineralizations collected from the Lagonegro Basin, the Albidona Fm., and the Apennine Carbonate Platform (separated for EAFS and MMFS provenance). The circles in panel a indicate veins collected from the Lagonegro Basin unit along the MMFS. In all panels, dashed circles indicate the different calcite clusters (1, 2, and 3). High confidence data are for clear fault kinematic indicators, whereas low confidence data are for the other mineralizations (see their tectonic interpretation in the Discussion section).

We performed carbonate clumped isotopes analyses on 75 samples from all 3 clusters (Table S1). Figure 6 displays the calculated precipitation temperatures ($T\Delta_{47}$) vs. the calculated $\delta^{18}O$ of the parental fluids. The vertical grey lines represent the maximum temperatures experienced by the host rocks during burial. We identify (Fig. 6a):

- Fluid group *a* characterized by parental fluids with $\delta^{18}O$ between -2 and -10 ‰ and $T\Delta_{47}$ between 10°and 30°C. These data were obtained from calcite mineralizations of cluster 1;
- Fluid group *b* characterized by parental fluids with $\delta^{18}O$ between -2 and -7 ‰ and $T\Delta_{47}$ between 40° and 80°C, all obtained from calcite mineralization of cluster 2;

- Fluid group *c* characterized by parental fluids with $\delta^{18}O$ between -1 and +16 ‰ and $T\Delta_{47}$ between 30° and 160°C, lower than maximum burial temperature experienced by the host rocks (120°C for the Albidona Fm. and Apennine Carbonate Platform; 160°C for the Lagonegro Basin unit), obtained from calcite mineralizations of cluster 3;
- Fluid group *d* characterized by parental fluids with $\delta^{18}O$ between +9 and +18 ‰ and $T\Delta_{47}$ between 150° and 220°C, higher than maximum burial experienced by the host rocks, obtained from calcite mineralizations of cluster 3;
- Fluid group *e* characterized by parental fluids with positive $\delta^{18}O$ between 1 and 5 ‰, $T\Delta_{47}$ between 100° and 120°C, obtained from calcite mineralizations of cluster 2.

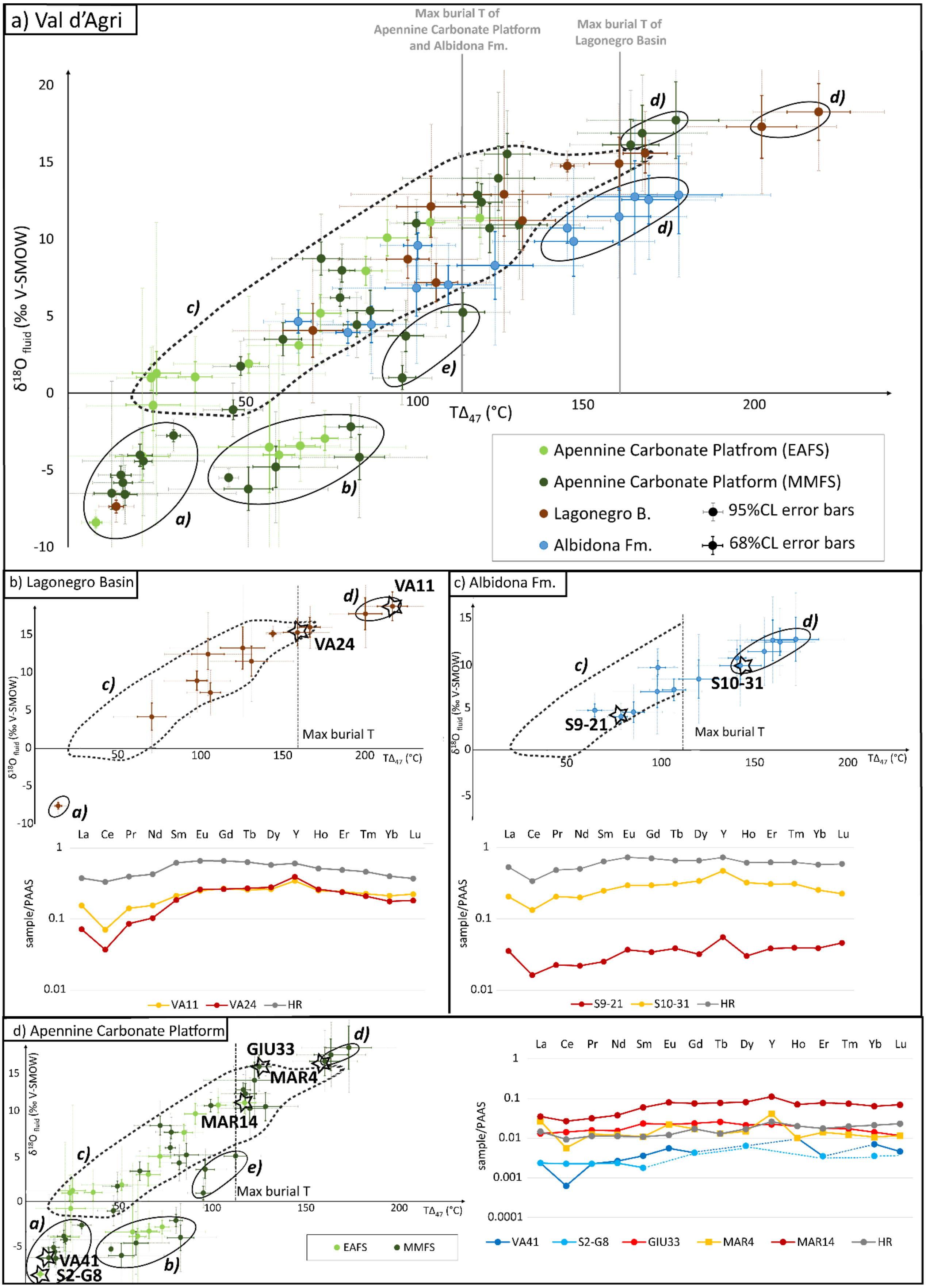

a) Val d'Agri
Max burial T of Apennine Carbonate Platform and Albidona Fm.
Max burial T of Lagonegro Basin
δ18O fluid (‰ V-SMOW)
TΔ47 (°C)
a)
b)
c)
d)
e)
Apennine Carbonate Platfrom (EAFS)
Apennine Carbonate Platform (MMFS)
Lagonegro B.
Albidona Fm.
95%CL error bars
68%CL error bars
b) Lagonegro Basin
VA11
VA24
Max burial T
sample/PAAS
La Ce Pr Nd Sm Eu Gd Tb Dy Y Ho Er Tm Yb Lu
VA11
VA24
HR
c) Albidona Fm.
S10-31
S9-21
S9-21
S10-31
HR
d) Apennine Carbonate Platform
GIU33
MAR4
MAR14
VA41
S2-G8
EAFS
MMFS
VA41
S2-G8
GIU33
MAR4
MAR14
HR

Fig. 6. a) $\delta^{18}O_{fluid}$ vs. $T\Delta_{47}$ plot for the fault-related calcite mineralizations, showing the recognized fluid groups (a, b, c, d, and e). The vertical grey lines represent the maximum temperatures experienced by the host rocks during burial. These burial temperatures are obtained by clay mineralogy as presented in Section 4.3. Error bars of $\delta^{18}O_{fluid}$ and $T\Delta_{47}$ are reported at both 68% (solid lines) and 95% (dotted lines) confidence level (CL; Table S1). b), c), d) $\delta^{18}O_{fluid}$ (‰ V-SMOW) vs. $T\Delta_{47}$ (°C) plot and Post Archean Australian shale (PAAS)-normalized REY trend (rare Earth elements + yttrium) of samples from Lagonegro Basin (b), Albidona Fm. (c), and Apennine Carbonate Platform (d). Stars and letters indicate the samples with the associated fluid group for which we analyzed REY elements. HR: host rock.

4.5. Rare-earth elements + Yttrium and Strontium isotopes

To provide additional constraints on parental fluids through REY and Sr isotope analyses, we selected samples representative of fluid groups a (VA41 and S2G8), c (MAR14, VA24, GIU33, and S9-21) and d (S11-11, MAR4, VA11, S10-15, S10-38, and S10-31; Table1).

Figure 6 compares the REY pattern of mineralizations normalized to PAAS (Post Archean Australian Shales, McLennan, 1989), with those of the corresponding host rocks. REY patterns of all veins and slickenfibers from the Lagonegro Basin unit and the Albidona Fm. mimic those of the host rocks, which are characterized by negative Ce and positive Y anomalies (Figs. 6b and c). Mineralizations are depleted in REE and are characterized by more pronounced Ce and Y anomalies than the host rocks (Table 1). This pattern is more evident for samples from fluid group *c* than those from group *d* (Table 1). The three analyzed fluid groups of the Apennine Carbonate Platform show different patterns of REY (Fig. 6d): group *a* is very depleted in REY elements; group *c* mimics the flat REY trend of the host rock and group *d* shows evident negative Ce as well as positive Eu and Y anomalies (Table 1).

Since the calcite veins and slickenfibers have low Rb concentrations (Table S3), the contribution of radiogenic ^{87}Sr is virtually negligible. Therefore, the measured $^{87}Sr/^{86}Sr$ ratio primarily reflects fluid interactions with rocks of specific stratigraphic ages and isotopic signatures. However, to account for the possible contamination of the Sr signature since the interaction with radiogenic fluids derived from dehydrated clays, we also calculated the $^{87}Sr/^{86}Sr$ ratio of the clay-rich Albidona Fm. rocks. This analysis revealed a particularly radiogenic ratio of 0.70895 for these rocks (Fig. 7).

In Figure 7, we compare the $^{87}Sr/^{86}Sr$ ratios of mineralizations with the expected values of the age of the corresponding host rocks (McArthur et al., 2001). Except for sample S9-21, which is characterized by a particularly high $^{87}Sr/^{86}Sr$ value, samples from fluid group *c* have $^{87}Sr/^{86}Sr$ consistent with the stratigraphic age of the host rocks. Samples of fluid groups *a* and *d* display Sr isotope disequilibrium with respect to the host rocks. Specifically, fluid group *a* exhibits a Pliocene-Pleistocene isotopic signature, in disequilibrium with the Late Triassic age of the host rocks. Fluid group *d* shows a Miocene isotopic signature in disequilibrium with the Eocene age of the host rocks (samples S10-15, S10-38), and an Early Cretaceous/Middle-Early Jurassic isotopic signature in disequilibrium with the Late Triassic age of the host rocks (S11-11 sample). Conversely, samples VA11, S10-31 and MAR4 of fluid group d show $^{87}Sr/^{86}Sr$ consistent with the host rocks (Fig. 7).

Table 1. Geochemical data for representative samples of different fluid groups

sample		Site & fault system	unit	mineralization type	$T\Delta_{47}$ (°C) (±95%CL)	$\delta^{18}O_{fluid}$ (‰ V-SMOW) (±95%CL)	$^{87}Sr/^{86}Sr$ (± se)	Sr (ppm)	ΣREY (ppm)	La*/ Lu*	Y/Ho	Eu/ Eu*	Ce/ Ce*	Y/Y*
fluid group a	VA41	11 MMFS	L. Triassic dolostones of Ap. Carb. Plat.	banded vein	13±36	-6.50 ±7.26	0.708994± 0.000009	23	0.35	0.51				
fluid group a	S2G8	5 EAFS	L. Triassic dolostones of Ap. Carb. Plat.	banded vein	8±4	-8.40 ±0.82	0.709101± 0.000008	63	0.44					
fluid group c	MAR 14	12 EAFS	L. Triassic-E. Cretaceous limestones of Ap. Carb. Plat.	Gently dipping (bed parallel) vein	120±13	11.36 ±2.63	0.707756± 0.000010	167	9.41	0.51	42.8	1.18	0.74	1.46
fluid group c	GIU 33	18 MMFS	M. Jurassic limestones of Ap. Crab. Plat.	gently dipping veins	128±14	15.53 ±2.82	0.707768± 0.000012	258	3.27	1.13	30	0.95	1.03	1.07
fluid group c	VA24	2 EAFS	L. Triassic limestones of Lagonegro B.	extensional slickenfibres	168±14	15.58 ±2.72	0.707899± 0.000007	1628	25.20	0.39	40.7	1.16	0.45	1.45
fluid group c	S9-21	6 EAFS	Eocene Albidona Fm.	compressional slickenfibers	82±8	3.93 ±1.51	0.709246± 0.000008	1431	5.78	0.77	50	1.24	0.53	1.78
fluid group d	S11-11	10 MMFS	L. Triassic dolostones of Ap. Carb. Plat.	transtensional slickenfibers	177±26	17.73 ±5.20	0.70723± 0.000009							
fluid group d	S10-31	7 EAFS	Eocene Albidona Fm.	extensional slickenfibers	147±24	9.84 ±4.73	0.707785± 0.000012	1296	45.53	0.91	40	1.09	0.65	1.43
fluid group d	MAR 4	23 MMFS	L. Triassic-E. Cretaceous limestones of Ap. Carb. Plat.	pinnate vein	164±18	16.13 ±3.54	0.707907± 0.000009	211	3.36	2.31	110	1.59	0.26	3.25
fluid group d	VA11	1 EAFS	Late Triassic limestones of Lagonegro B.	transtensional slickenfibers	219±19	18.27 ±3.82	0.708066± 0.000009	513	32.07	0.69	37.2	1.04	0.46	1.34
fluid group d	S10-15	7 EAFS	Eocene Albidona Fm.	extensional slickenfibres	169±19	12.56 ±3.88	0.708745± 0.000008							
fluid group d	S10-38	7 EAFS	Eocene Albidona Fm.	transtensional slickenfibers	178±27	12.87 ±5.36	0.708776± 0.000012							

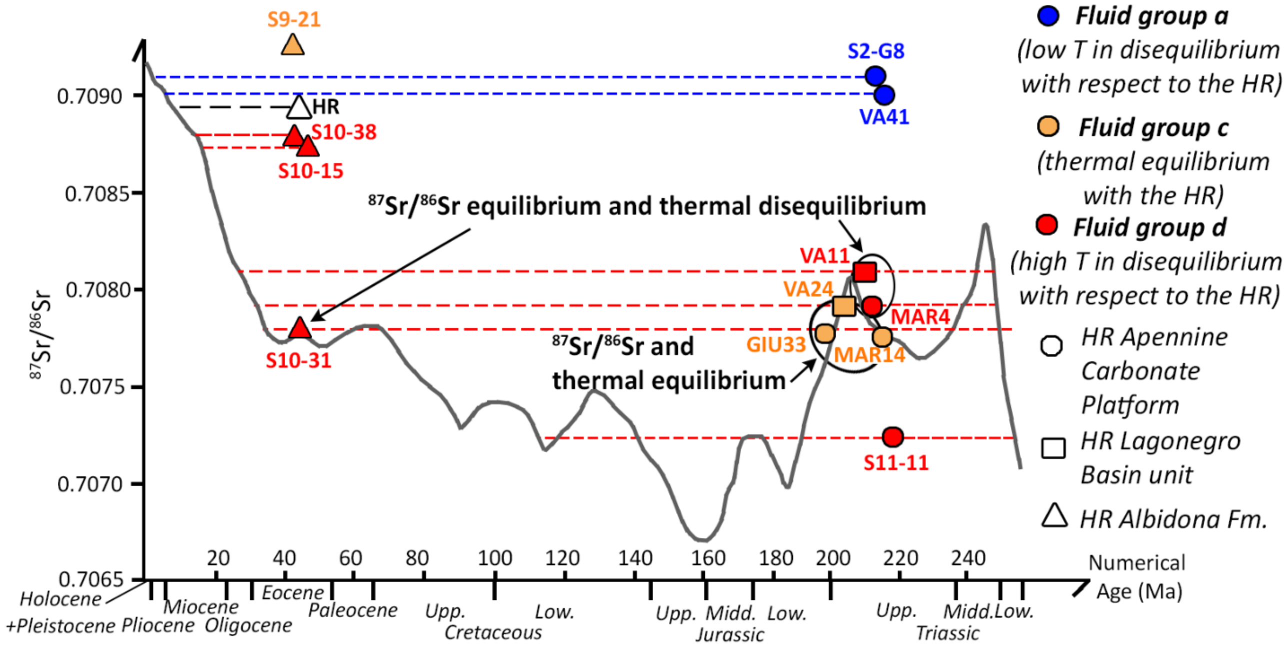

Fig. 7. $^{87}Sr/^{86}Sr$ values of fault-related calcite mineralizations compared with the Sr isotope evolution of seawater by McArthur et al. (2001). The age of the host rocks is from Palladino et al. (2023). Samples are distinguished by the host rock (HR) lithology and identified fluid groups (Table 1). The $^{87}Sr/^{86}Sr$ value of the Albidona Fm. rock are shown in the plot to highlight the influence of radiogenic strontium on syn-tectonic calcite mineralizations.

5. Discussion

5.1. Parental fluid origin and evolution

Calcite mineralizations of cluster 1 is characterized by $\delta^{13}C$ values comprised between -2 ‰ and -12 ‰ (Fig. 5), indicating a contribution of light carbon derived by oxidation of organic matter (e.g., Sharp, 2017). This cluster precipitated from fluids with a $\delta^{18}O$ between -2 and -10‰, and a $T\Delta_{47}$ between 10° and 30°C (group *a*; Fig. 6a). These values are consistent with the present-day composition, of meteoric water from the Val d'Agri area (i.e., $\delta^{18}O$ -8‰, and T between 18° and 30°C; Italiano et al., 2001). Thus, we interpret that calcite of cluster 1 precipitated from meteoric waters interacting with shallow soil organic carbon before their infiltration at depth.

Calcite mineralizations of cluster 2 show $\delta^{13}C$ values similar to that of their host rocks, and $\delta^{18}O$ values mostly between +14 ‰ and +21 ‰ (Fig. 5), in disequilibrium with respect to the host rocks. Calculated parental fluid compositions of this cluster have $\delta^{18}O$ values between -2 and -7 ‰, hence retaining a meteoric water signature, but with a $T\Delta_{47}$ between 40° and 80°C (group *b*; Fig. 6a). Since the dissolved inorganic carbon is a trace component of water, the carbon isotope ratios can be rapidly buffered by the host rocks, even with a short residence time. Conversely, oxygen, a major component of water, requires a longer residence time or low water/rock ratios to be buffered (Sharp, 2017). Therefore, we conclude that the fluid source of calcite cluster 2 consists of meteoric water that infiltrated at depth and warmed up with a limited isotope exchange with the host rocks. We observe that samples S11-5, MAR27, and MAR30 (Table S1), from the calcite cluster 2, precipitated from fluids with $\delta^{18}O$ values between 1 and 5 ‰, and $T\Delta_{47}$ between 100° and 120°C (group *e*; Fig. 6a). Since these high temperatures are apparently at odds with the relatively low $\delta^{18}O$ values, we interpret them as due to the mixing of warm fluids (T >> 100°C) with colder, infiltrated meteoric water.

Calcite cluster 3 exhibits $\delta^{13}C$ and $\delta^{18}O$ values almost equal to the host rocks (Fig. 5). The calculated $\delta^{18}O$ values of parental fluids > -1 ‰ (groups *c* and *d* in Fig. 6a) indicate either a low fluid/rock ratio, or a long-term fluid-host rock interaction with higher fluid/rock ratios (Sharp, 2017). For these fluids, we observe a wide range of $T\Delta_{47}$ and oxygen isotope values, demonstrating a wide variability in water-rock interaction, and/or in the mixing of different end-member fluids. The precipitation temperatures of 200°-220°C of some mineralizations from the Lagonegro Basin unit as well as 150°-180°C of some mineralizations from the

Apennine Carbonate Platform/Albidona Fm. (Fig. 6a) are significantly higher than the maximum burial temperature experienced by the host rocks (140°-160°C for the Lagonegro Basin unit and 110°-120°C for Albidona Fm. and Apennine Carbonate Platform, estimated by the thermal modeling of Aldega et al., 2003 and Corrado et al., 2005 and integrated with our new XRD data presented above).

Summarizing, parental fluids of calcite cluster 3 are either in thermal equilibrium (group *c*) or disequilibrium (group *d*) with respect to the maximum burial temperatures of the host rocks. The sources of fluid group *c* could include: meteoric waters isotopically buffered and in thermal equilibrium with the host rocks; water expelled during the smectite to illite transformation reaction; and formation waters trapped within shaly interlayers and expelled due to compaction (e.g., Smeraglia et al., 2020). In contrast, the high temperatures of fluid group *d* require a source deeper than the host rocks. By assuming a geothermal gradient of 30°C/km, and a surface temperature of 10°C, as proposed by Aldega et al. (2003) and Corrado et al. (2005), the $T\Delta_{47}$ of 220°C from mineralizations within the Lagonegro unit is consistent with an origin of parental fluids from depths of ~ 7 km. This corresponds to the burial depths of the Apulian Carbonate Platform both during orogenic and post-orogenic phases. Indeed, considering a post-orogenic exhumation of ~4-5 km (Aldega et al., 2003) for the top of the Apulian Carbonate Platform, which is currently located at depths of 2-3 km beneath the Val d'Agri Basin (Butler et al., 2004; Hager et al., 2021), its maximum can be estimated to be approximately 6-8 km. Therefore, fluids with temperatures ranging from 150°-180°C that permeated the Albidona Fm. and Apennine Carbonate Platform probably derived from rocks at a depth of ~4.5-5.5 km. They could be derived from the Lagonegro Basin unit or the Apulia Carbonate Platform, depending on the extent of rock exhumation at the time of calcite precipitation.

These interpretations are also supported by REY and Sr isotope. Samples of calcite cluster 1 are strongly depleted in REY (Fig. 6d), consistent with precipitation from meteoric water (fluid group *a*; Mcleannan, 1985). On the other hand, most samples of calcite cluster 3 are depleted in LREE elements (La*/Lu*< 0.8), are characterized by moderately negative Ce and positive Y anomalies, and show a Y/Ho ratio between 30 and 50 (Table 1). This is consistent with seawater inheritance (Mcleannan, 1985; Tostevin et al., 2016) from the sedimentation environment of the carbonate host rocks and with a long-term fluid-rock interaction. The lack of Ce and Y anomalies in samples GIU33, S10-31, and VA11 of calcite cluster 3 may be due to contamination with clay minerals. Clays containing high concentrations of REY with an almost flat trend (Fig. 6) would dilute any possible anomalies (e.g., Tostevin et al., 2016). Additionally, the MAR4 sample (fluid group *d*) is enriched in LREE (La*/Lu*=2.31) and shows a pronounced Eu positive anomaly and Y/Ho = 110 (Table 1), likely resulting from thermochemical sulphate reduction experienced by hydrocarbon-rich fluids (Jiang et al., 2015). This is consistent with the proposed origin for fluid group *d* from the Apulian Carbonate Platform, where the hydrocarbons are trapped.

Furthermore, samples S10-31, VA11, and MAR4 from fluid group *d* and samples VA24, GIU33, and MAR14 from fluid group *c* show a Sr isotope signatures consistent with their host rocks, whereas samples S10-38, S10-15, S11-11 from fluid group *d* and samples S2-G8, VA41 from fluid group *a* are not consistent with the stratigraphic age of the host rocks (Fig. 7). Sample S9-21 (group *c*) shows anomalously high $^{87}Sr/^{86}Sr$ values, which we interpret as due to a long-term interaction of parental fluid with the clay-rich Albidona Fm. host rock rich in radiogenic Sr (Fig. 7). The Pliocene-Pleistocene Sr isotope signatures of samples from fluid group *a* (Fig. 7) are consistent with precipitation from meteoric fluids, which chemically interacted with shallow Pliocene-Pleistocene continental deposits (0.70907-0.70910; Mancini et al., 2007). The Sr isotope ratios of samples from fluid group *c*, consistent with the stratigraphic age of the host rocks, confirm the host-rock buffering of these fluids (Fig. 7). The samples of group *d*, precipitated from hot fluids in thermal disequilibrium with the host rocks, suggest a fluid origin deeper than the host rocks. Consequently, we interpret the Miocene-age Sr isotope signature of samples S10-15 and S10-38 (Fig. 7) as due to the fluid interaction with the Irpinia mélange or the top of the Apulian Carbonate Platform, and the Early Cretaceous/Middle-Early Jurassic Sr isotope signature of sample S11-11 (Fig. 7), as due to the interaction with the middle portion of the Apulian Carbonate Platform (Fig. 1b). Possibly, the apparent Sr isotope ratio of samples VA11, MAR4, and S10-31 (fluid group *d*) consistent with the stratigraphic age of the host rocks (Fig. 7) could be due to the interaction with Late Triassic dolostones of the Apulian Carbonate Platform.

5.2. Tectonic interpretation of fault-related mineralizations

The studied mineralizations, sampled along the high-angle post-orogenic extensional faults pertaining either to the EAFS or to the MMFS, can be attributed with different levels of confidence to orogenic compressional or post-orogenic extensional tectonics (Table 2). Calcite samples forming kinematic indicators as slickenfibers, sigmoidal tension gashes, and pinnate veins are interpreted with high confidence as syn-kinematic (Roberts & Holdsworth, 2022). Based on their kinematics, these samples can be confidently associated with orogenic compressional or post-orogenic extensional faulting. On the contrary, the tectonic origin of steeply and gently dipping veins as well as banded and stockwork veins, which are not associated with straightforward kinematic indicators, can interpret with a low confidence level.

The attitude of steeply dipping veins is consistent with the shear sense of nearby post-orogenic extensional faults, suggesting a kinematic relationship, and is compatible with the present-day extensional stress regime (Mariucci and Montone, 2020). Furthermore, these veins are not cut or displaced by structures associated with orogenic compressional phases, reinforcing their association with the post-orogenic extensional phase. Hence, we interpret them as products of the post-orogenic extensional phase. The banded veins, which cut across bed interfaces and extensional faults/fractures (Fig. S1), likely formed during the youngest crack and seal episodes of the post-orogenic extension (Uysal et al., 2011). The gently dipping veins have a geometry incompatible with the kinematics of high-angle extensional faults and are generally subparallel to bedding. In some cases, these veins are also cut by high-angle extensional faults (Fig. 2d). Since this type of vein is frequent in fold-and-thrust belts and is generally associated with the early compressive phases and related fluid overpressures (Jessell et al., 1994; Sibson, 2020), we interpret them as products of the orogenic compressional phase. Stockwork veins are generally related to rapid fluid depressurization of pressurized fluids during faulting (Sibson, 2000; Bons et al., 2022). Here, we interpret them as due to compressional tectonics, when observed at the footwall of reverse faults, or to extensional tectonics when observed at the footwall of extensional-transtensional faults. Supporting this interpretation, at the microscale, stockwork veins observed near thrust faults (samples GIU22, GIU33, and VA25; Tables S1-S2) commonly display mutual crosscutting relationships with seismogram-like stylolites, interpreted as syn-orogenic by Manniello et al.

(2023), whereas those sampled near extensional faults (sample VA17; Table S1) cut across such stylolites (Fig. 3).

In the Val d'Agri, both post-orogenic extensional and orogenic compressional faulting was preceded by rift-related and foreland flexure-related extensional faulting (Mazzoli et al., 2001; Patacca & Scandone, 2007; Schirripa Spagnolo et al., 2024). Thus, in principle, we cannot entirely rule out the possibility that some of the steeply dipping veins are inherited from such pre-orogenic tectonic stages. However, we consider them to be too rare to affect the robustness of our fluid circulation model, for the following reasons: 1) background veins, far from post-orogenic extensional faults, are very rare and generally parallel to bedding (i.e., not associated with extensional faulting); 2) the rare Mesozoic syn-sedimentary faults, recognized only in the Lagonegro Basin unit on stratigraphic grounds, were only weakly reactivated under contraction (Mazzoli et al., 2001); 3) no double inversion (first contractional and then extensional) of pre-orogenic faults has been recognized or described in the literature.

Table 2. Synthesis of structural-geochemical results characteristic of each fluid group

Fluid group and source	**Tectonic unit and fault system**	**Myneralization type associated with post-orogenic tectonics**	**Myneralization type associated with orogenic tectonics**	**Micro-structural assemblage**	**Calcite cluster**	**$\delta^{18}O_{fluid}$ (‰ V-SMOW)**	**$T\Delta_{47}$ (°C)**	**REY trend and anomalies**	**$^{87}Sr/^{86}Sr$ ratio**
(a) Meteoric water	Lagonegro Basin and Apennine Carbonate Platform (both along EAFS and MMFS)	-banded veins (low confidence) - extensional slickenfibers (high confidence) -steeply dipping veins (low confidence)	-	Blocky and elongated texture, thin twinning, no luminescence	(1)	-3 to -9	10-30	Depleted in REY elements	Pliocene-Pleistocene Sr isotope signature
(b) Meteoric water with low residence time	Apennine Carbonate Platform (both along EAFS and MMFS)	-steeply dipping veins (low confidence) - extensional slickenfibers (high confidence)	- gently dipping (bed parallel) veins (low confidence)	Blocky texture, thin twinning, no luminescence	(2)	-3 to -7	50-80	-	-
(c) Host rock-buffered fluid (long residence time)	Albidona Fm., Lagonegro Basin, and Apennine Carbonate Platform (both along EAFS and MMFS)	- extensional slickenfibers (high confidence) - extensional tension gash (high confidence) - steeply dipping veins (low confidence)	- gently dipping (bed parallel) veins (low confidence) -compressional slickenfibers (high confidence) - compressional tension gash (high confidence) -stockwork veins near compressional faults (low confidence)	Blocky texture, thin and thick twinning; no luminescence or luminescence with same intensity of the HR one	(3)	-1 to 16	70-120 for Apennine CarbonatePlatform and Albidona Fm., 100-170 for Lagonegro Basin unit.	moderate Ce, Y anomalies; Y/Ho <50	Sr isotope signature in equilibrium with respect to the stratigraphic age of the host rocks
(d) High T fluid (Apulian Carbonate Platform origin)	Albidona Fm., Lagonegro Basin, and MMFS Apennine Carbonate Platform	- pinnate veins (high confidence) - stockwork veins near extensional faults (low confidence) - extensional slickenfibers (high confidence)		Blocky texture thin and thick twinning, no luminescence or luminescence more intense than HR	(3)	10 to 18	200-220 for Lagonegro Basin unit 150-180 for Apennine Carbonate Platform and Albidona Fm.	moderate Ce, Y anomalies; Y/Ho > 100	Late Triassic, Early Cretaceous/ Middle Jurassic, Miocene Sr isotope signature
(e) Mixing between high T fluids and meteoric water	MMFS Apennine Carbonate Platform	- extensional slickenfibers (high confidence)		Blocky texture; thin twinning; no luminescence	(2)	1 to 5	100-120	-	-

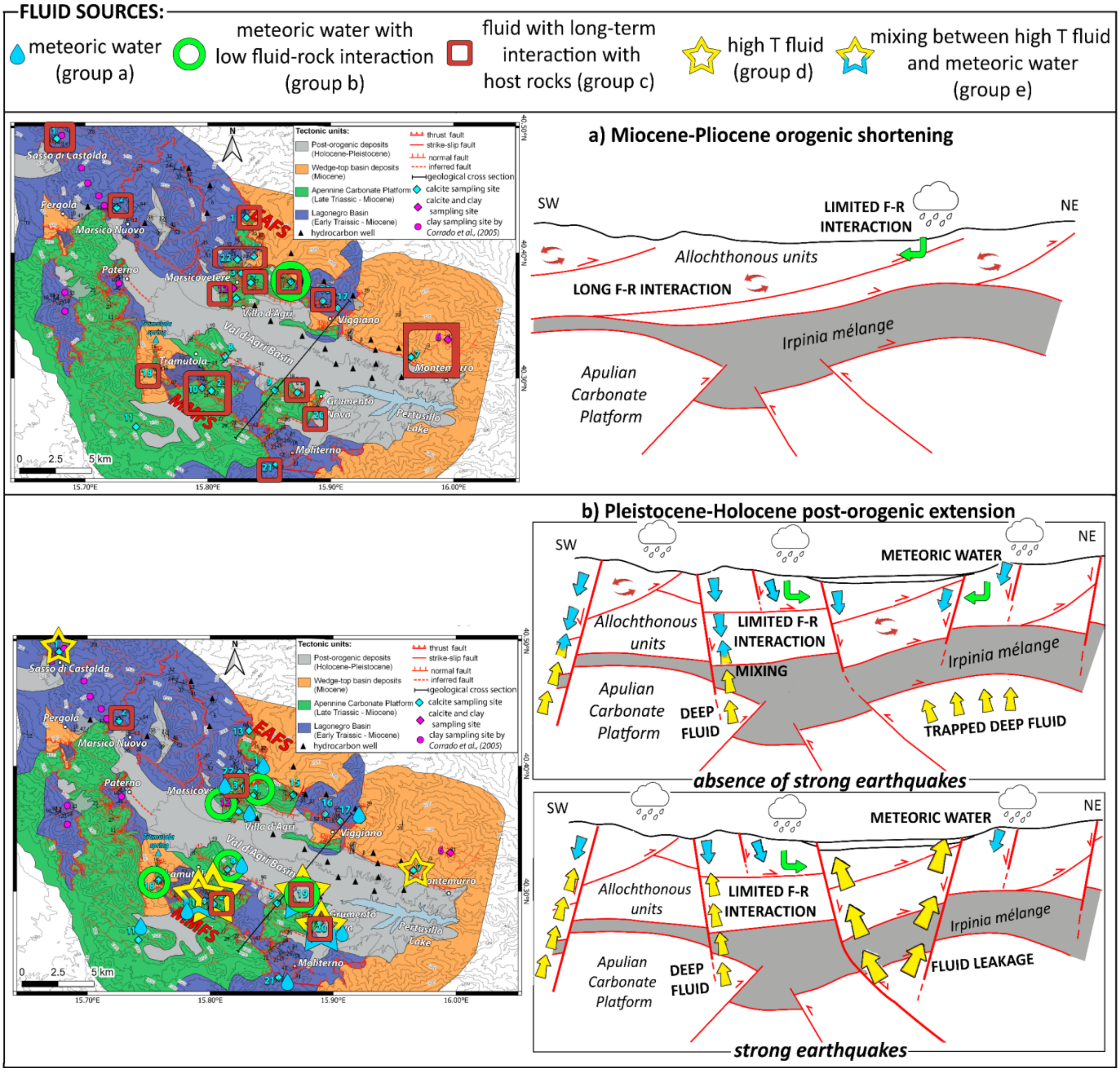

Fig. 8. Structural map of the Val d'Agri Basin (to the left) with spatial distribution of parental fluid groups involved during the Miocene-Pliocene orogenic (panel a) or the Pleistocene-Holocene post-orogenic (panel b) tectonic phases. Schematic models of fluid flow/distribution are provided for each phase. Notice that during the post-orogenic phase, fluid circulation differs during strong earthquakes.

5.3. Spatiotemporal fluid circulation

Based on the results discussed above, and synthesized in Table 2, mineralizations associated with orogenic shortening precipitated from fluids in chemical and thermal equilibrium with the host rocks (group *c*; Table 2). This indicates a compartmentalized fluid-circulation system (e.g., Beaudoin et al., 2023) involving intraformational fluids and/or meteoric fluids completely buffered by the host rocks during the orogenic compressional tectonics (Fig. 8a). This scenario is consistent with the interpretation of Gabellone et al. (2013) for calcite veins from the Val d'Agri Basin, and with other case studies from the central Italian Apennines (e.g., Smeraglia et al., 2020; Curzi et al., 2024) and other fold-and-thrust worldwide belts (e.g., Beaudoin et al., 2023).

Mineralizations associated with post-orogenic extension are characterized by parental fluids belonging to all groups (*a*, *b*, *c*, *d*, and *e*; Table 2; Fig. 8b). Cold fluids of groups *a* and *b* are associated with the infiltration of meteoric water, a common process within rocks undergoing dilation in extensional settings (Sibson, 2000; Doglioni et al., 2014; Curzi et al., 2024). Host-rock buffered fluids of group *c*, characterized by geochemical and thermal equilibrium with the host rocks, suggest near-surface fluid circulation enhanced by rapid dilation and increased porosity of rocks (Sibson 2000; Curzi et al., 2024). Hot fluids of group *d*, in geochemical equilibrium and in thermal disequilibrium with the host rocks, are consistent with the ascent of fluids from deeper structural levels during extensional faulting (Sibson 2000; Curzi et al., 2024). The proposed fluid source is the Apulian Carbonate Platform, which is separated from shallower units by the impermeable Irpinia mélange. The hot fluids of group *e* are interpreted as a mixing of fluid groups *a* and *d,* and therefore indicate structural connections between the Apulian Carbonate Platform and the near surface.

Spatial distribution of fluid groups within the Val d'Agri Basin during post-orogenic extensional tectonics (Fig. 8b) highlights the key role played by the tectonic mélange on fluid flow. Where the mélange is thin, mainly below the MMFS and site 1 (Butler et al., 2004; Catalano et al., 2004), the fluid systems hosted in the units above and below the mélange were frequently connected by extensional-transtensional faults, which could easily breach the mélange (Candela et al., 2015; Schirripa Spagnolo et al., 2024). This is testified by the wide occurrence of mineralizations precipitated from fluid groups *d* and *e* (Fig. 8b). In the same areas, the occurrence of mineralizations from groups *a*, *b*, and *c* testifies to a spatial and/or temporal lack of connection across the Irpinia mélange. The described fluid circulation system is consistent with the present-day natural leakage of hydrocarbons along the MMFS and in other localities of the Val d'Agri Basin (e.g., Colangelo et al., 2005; Beaubien et al., 2023).

Conversely, in areas characterized by thicker tectonic mélange (mainly below the EAFS; Fig. 8), the fluid systems hosted in the units above and below the mélange were generally compartmentalized, allowing the formation and preservation of the hydrocarbon trap below the Irpinia mélange (Hager et al., 2021). This process is consistent with widespread calcite precipitation from meteoric waters (groups *a* and *b*; Fig. 8b) and occasionally from host-rock buffered fluids (group *c*; Fig. 8b). It is also true, however, that at sampling site 7 (EAFS; Fig. 8b), below which the mélange thickness is > 1 km and productive oil reservoirs are located (Hager et al., 2021), mineralizations precipitated from hot fluids originated from the Apulian Carbonate Platform (fluid group *d*). This exceptional case might have been ruled by the valve behavior of major regional faults. Specifically, during strong seismic events, these faults may have allowed the hard-linkage, across the mélange, between shallow and deep structures and the related upward leakage of fluids (e.g., Sibson , 2000). The occurrence of the productive hydrocarbon reservoir below the EAFS indicates that, over the long term, extensional faulting has not substantially interrupted the continuity of the Irpinia mélange. However, we propose that (likely strong) earthquakes were able to episodically breach the mélange, allowing the ascent of fluids from the Apulian Carbonate Platform (Fig. 8b).

Similar occasional ascents of trapped fluids from hydrocarbon reservoirs due to seismic fault-valve action were described in the literature (e.g., Jin et al., 2008), and explained by the plastic-to-brittle transition of seal rocks with higher strain rates (e.g., Cheng & Ben-Zion, 2019). The role of earthquakes in controlling fluid upwelling from the Apulian Carbonate Platform is also emphasized by some studies suggesting that the initiation of the natural emissions of hydrocarbons near Tramutola village was related to the 1857 Mw7.1 earthquake (Colangelo et al., 2005).

6. Conclusions, implications and recommendations

The paleo-fluid circulation within the Val d’Agri Basin was significantly influenced by the prevailing tectonic regime (compressive vs. extensional), the stratigraphic-structural architecture, and the occurrence of seismic events. During orogenic shortening, the progressive stacking of multiple thrust sheets substantially prevented vertical fluid circulation. Conversely, during the ongoing post-orogenic extension, the vertical circulation of fluids was predominantly controlled by the compartmentalization efficiency of the Irpinian mélange. This efficiency was improved by the increased thickness of the mélange but was compromised by faulting and associated seismic events, which promoted the upward ascent of deep fluids.

These results highlight the importance of considering the regional tectonic setting for hydrocarbon extraction, subsurface gas storage, or earthquake hazard mitigation. In active compressional settings, an impermeable horizon is more likely to remain intact under natural conditions, implying that fluids injecting below the impermeable horizon during extraction activities could significantly increase fluid pressure, potentially inducing earthquakes.

In active post-orogenic extensional settings, fluid accumulation is related to the orogenic architecture where thrust sheets may act as sealing horizons. However, active extensional faulting and associated seismic events may threaten the integrity of sealing horizons. The presence of sealing horizons and fluid traps, combined with the man-induced variations of pore fluid pressure, could also cause earthquakes, as observed in the Val d'Agri Basin (Improta et al., 2017; Hager et al., 2021). During extensional faulting, particularly in the case of strong seismic events, faults could serve as conduits for the ascent of pressurized fluids, which could be polluting or dangerous. This process will be influenced by the thickness of the sealing horizon(s).

In conclusion, hydrocarbon extraction and subsurface gas storage in seismically active areas present unique challenges and risks that must be addressed to reduce potential seismic or environmental hazards. Therefore, in geological settings comparable to the Val d'Agri Basin, where exploitation or storage activities are ongoing (e.g., the Pannonian Basin in Hungary, Czauer and Madl-Szonyi, 2011, the Bohai Bay Basin in China, Song et al., 2022, and the Nispiro Field in Mexico, Bourdet et al., 2010), we recommend rigorous seismic monitoring and risk assessment.

7. Declaration of Generative AI and AI-assisted technologies in the writing process

During the preparation of this work the author(s) used ChatGPT in order to improve readability and fluency. After using this tool/service, the author(s) reviewed and edited the content as needed and take(s) full responsibility for the content of the publication.

8. Acknowledgements

The authors thanks Jean-Philippe Avouac (editor of EPSL), Nicolas Beaudoin, and an anonymous reviewer for their constructive feedback and comments that have helped improve this manuscript. We thanks Actalabs team for REY analyses, Madalina Jaggi , Stewart Bishop, Reto Wijker, Nathan Looser, Alexander Johannes Clark, and Ricarda Rosskopf for assistance with clumped isotopes analysis, Domenico Mannetta for thin section preparation, Sara Ronca, Marco Brandano, Barbara Marchesini, and Valeria Ruscitto for assistance with optical and cathodoluminescence analysis, Vincenzo Moretto for assistance with XRD analysis, Canio Maniello, Fabio Olita, and Lorenzo Petracchini for help during field work. Funding by Sapienza Progetti di Ateneo 2020 (L. Aldega), 2021 (E. Carminati), and 2023 (G. Schirripa Spagnolo), Sapienza Progetti per la Mobilità Estera di dottorandi (G. Schirripa Spagnolo). Funding by MASE (the Italian Ministry of the Environment and Energy Security) to the Dipartimento di Scienze della Terra-Sapienza Università di Roma and IGAG-CNR for the project "Circolazione di fluidi nelle zone di faglia della Val d'Agri " is acknowledged. MASE is also thanked for allowing publication of the data acquired in the project. S.Bernasconi acknowledges funding from Swiss SNF project 200021_169849.

9. References

1. Anderson, N. T., Kelson, J. R., Kele, S., Daëron, M., Bonifacie, M., Horita, J., Mackey, T. J., John, C.M., Kluge T., Petschnig, P., Jost, A.B., Huntington, K. W, Bernasconi, S.M., & Bergmann, K. D. (2021). A unified clumped isotope thermometer calibration (0.5–1,100 C) using carbonate-based standardization. Geophysical Research Letters, 48(7), e2020GL092069. https://doi.org/10.1029/2020GL092069
2. Aldega, L., Corrado, S., Giampaolo, C., & Mazzoli, S. (2003). Studio della mineralogia delle argille per la ricostruzione dei carichi tettonico/sedimentari; esempi dalle Unita Lagonegresi e Liguridi della Lucania sud-occidentale (Appennino Meridionale). *Bollettino della Società geologica italiana*, *122*(2), 203-216.
3. Beaubien, S. E., Spagnolo, G. S., Ridolfi, R. M., Aldega, L., Antoncecchi, I., Bigi, S., Billi, A., & Carminati, E. (2023). Structural control of gas migration pathways in the hydrocarbon-rich Val d'Agri basin (Southern Apennines, Italy). *Marine and Petroleum Geology*, *154*, 106339. https://doi.org/10.1016/j.marpetgeo.2023.106339
4. Beaudoin, N. E., Lacombe, O., Hoareau, G., & Callot, J. P. (2023). How the geochemistry of syn-kinematic calcite cement depicts past fluid flow and assists structural interpretations: a review of concepts and applications in orogenic forelands. *Geological Magazine*, *159*(11-12), 2157-2190. https://doi.org/10.1017/S0016756822001327
5. Bello, S., Lavecchia, G., Andrenacci, C., Ercoli, M., Cirillo, D., Carboni, F., Barchi M. R., Brozzetti, F., (2022). Complex trans-ridge normal faults controlling large earthquakes. Scientific Reports, 12(1), 1-20. https://doi.org/10.1038/s41598-022-14406-4
6. Benedetti, L., Tapponnier, P., King, G. C. P., Piccardi, L., (1998). Surface rupture of the 1857 southern Italian earthquake? *Terra Nova*, 10(4), 206-210. https://doi.org/10.1046/j.1365-3121.1998.00189.x
7. Bons, P. D., Cao, D., De Riese, T., González-Esvertit, E., Koehn, D., Naaman, I., Sachaou, T., Tian, H., & Gomez-Rivas, E. (2022). A review of natural hydrofractures in rocks. *Geological Magazine*, *159*(11-12), 1952-1977. https:// doi.org/10.1017/S0016756822001042
8. Borraccini, F., De Donatis, M., Di Bucci, D., Mazzoli, S., 2002. 3D model of the active extensional fault system of the high Agri River valley, Southern Apennines, Italy. J. Virtual Expl, 6, 1-6.
9. Bourdet, J., Pironon, J., Levresse, G., & Tritlla, J. (2010). Petroleum accumulation and leakage in a deeply buried carbonate reservoir, Níspero field (Mexico). *Marine and Petroleum Geology*, *27*(1), 126-142. https://doi.org/10.1016/j.marpetgeo.2009.07.003

10. Brozzetti, F., (2011). The Campania-Lucania Extensional Fault System, southern Italy: A suggestion for a uniform model of active extension in the Italian Apennines. Tectonics, 30(5). https://doi.org/10.1029/2010TC002794

11. Butler, R. W. H., Mazzoli, S., Corrado, S., De Donatis, M., Di Bucci, D., Gambini, R., Naso G., Nicolai C., Scrocca D., Shiner P., Zucconi, V. (2004). Applying thick-skinned tectonic models to the Apennine thrust belt of Italy—Limitations and implications. *Thrust Tectonics and Hydrocarbon Systems*, 647-667. https://doi.org/10.1306/M82813C34

12. Caine, J. S., Evans, J. P., & Forster, C. B. (1996). Fault zone architecture and permeability structure. *Geology*, *24*(11), 1025-1028. https://doi.org/10.1130/0091-7613(1996)024<1025:FZAAPS>2.3.CO;2

13. Candela, S., Mazzoli, S., Megna, A., & Santini, S. (2015). Finite element modelling of stress field perturbations and interseismic crustal deformation in the Val d'Agri region, southern Apennines, Italy. *Tectonophysics*, *657*, 245-259. http://dx.doi.org/10.1016/j.tecto.2015.07.011 0040-1951

14. Catalano, S., Monaco, C., Tortorici, L., Paltrinieri, W., & Steel, N. (2004). Neogene-Quaternary tectonic evolution of the southern Apennines. *Tectonics*, *23*(2).https://doi.org/10.1029/2003TC001512

15. Chiodini, G., Cardellini, C., Di Luccio, F., Selva, J., Frondini, F., Caliro, S., Rosiello, A., Beddini, G., & Ventura, G. (2020). Correlation between tectonic CO2 Earth degassing and seismicity is revealed by a 10-year record in the Apennines, Italy. *Science Advances*, *6*(35), eabc2938. DOI: 10.1126/sciadv.abc2938

16. Cello, G., Gambini, R., Mazzoli, S., Read, A., Tondi, E., & Zucconi, V. (2000). Fault zone characteristics and scaling properties of the Val d'Agri Fault System (Southern Apennines, Italy). *Journal of Geodynamics*, *29*(3-5), 293-307. https://doi.org/10.1016/S0264-3707(99)00043-5

17. Cheng, Y., and Ben-Zion, Y., (2019), Transient brittle ductile transition depth induced by moderate large earthquakes in southern and Baja California: Geophysical Research Letters, v. 46, p. 11,109 11,117. https://doi.org /10.1029/2019GL084315

18. Colangelo, G., Heinicke, J., Koch, U., Lapenna, V., Martinelli, G., & Telesca, L. (2005). Results of gas flux records in the seismically active area of Val d'Agri (Southern Italy). *Annals of Geophysics*, 48(1).

19. Colangelo, G., Heinicke, J., Lapenna, V., Martinelli, G., & Mucciarelli, M. (2007). Investigating correlations of local seismicty with anomalous geoelectrical, hydrogeological and geochemical signals jointly recorded in Basilicata Region (Southern Italy). *Annals of Geophysics*, 50, 527-538. http://hdl.handle.net/2122/3866

20. Corrado, S., Aldega, L., Di Leo, P., Giampaolo, C., Invernizzi, C., Mazzoli, S., Zattin, M., (2005). Thermal maturity of the axial zone of the Southern Apennines fold-and thrust-belt (Italy) from multiple organic and inorganic indicators. *Terra Nova, 17 (1), 56-65.* https://doi.org/10.1111/j.1365-3121.2004.00584.x
21. Cucci, L., Pondrelli, S., Frepoli, A., Mariucci, M. T., Moro, M., (2004). Local pattern of stress field and seismogenic sources in the Pergola–Melandro basin and the Agri valley (Southern Italy). *Geophysical Journal International*, 156(3), 575-583. https://doi.org/10.1111/j.1365-246X.2004.02161.x
22. Curzi, M., Aldega, L., Billi, A., Boschi, C., Carminati, E., Vignaroli, G., Viola, G., & Bernasconi, S. M. (2024). Fossilchemical-physical (dis) equilibria between paleofluids and host rocks and their relationship to the seismiccycle and earthquakes. *Earth-Science Reviews*, 104801. https://doi.org/10.1016/j.earscirev.2024.104801
23. Czauner, B., & Madl-Szonyi, J. (2011). The function of faults in hydraulic hydrocarbon entrapment: Theoretical considerations and a field study from the Trans-Tisza region, Hungary. *AAPG bulletin*, *95*(5), 795-811. https://doi.org/10.1306/11051010031
24. D’Adda, P., Longoni, R., Magistroni, C., Meda, M., Righetti, F., Cavozzi, C., Nestola, Y., & Storti, F. (2017). Extensional reactivation of a deep transpressional architecture: Insights from sandbox analogue modeling applied to the Val d’Agri basin (Southern Apennines, Italy). *Interpretation*, 5(1), SD55-SD66. https://doi.org/10.1190/INT-2016-0078.1
25. Doglioni, C., Barba, S., Carminati, E., & Riguzzi, F. (2014). Fault on–off versus coseismic fluids reaction. *Geoscience Frontiers*, *5*(6), 767-780. https://doi.org/10.1016/j.gsf.2013.08.004
26. Ellsworth, W. L. (2013). Injection-induced earthquakes. *science*, *341*(6142), 1225942. 10.1126/science.1225942
27. Faulkner, D. R., Jackson, C. A. L., Lunn, R. J., Schlische, R. W., Shipton, Z. K., Wibberley, C. A. J., & Withjack, M. O. (2010). A review of recent developments concerning the structure, mechanics and fluid flow properties of fault zones. *Journal of Structural Geology*, *32*(11), 1557-1575. https://doi.org/10.1016/j.jsg.2010.06.009
28. Gabellone, T., Gasparrini, M., Iannace, A., Invernizzi, C., Mazzoli, S., & D'Antonio, M. (2013). Fluid channeling along thrust zones: the Lagonegro case history, southern Apennines, Italy. *Geofluids*, *13*(2), 140-158. https://doi.org/10.1111/gfl.12020

29. Giano, S. I., Maschio, L., Alessio, M., Ferranti, L., Improta, S., Schiattarella, M., 2000. Radiocarbon dating of active faulting in the Agri high valley, southern Italy. Journal of Geodynamics, 29(3-5), 371-386. https://doi.org/10.1016/S0264-3707(99)00058-7
30. Grunau, H. R. (1987). A worldwide look at the cap-rock problem. *Journal of Petroleum Geology*, *10*(3), 245-265. https://doi.org/10.1111/j.1747-5457.1987.tb00945.x
31. Hager, B. H., Dieterich, J., Frohlich, C., Juanes, R., Mantica, S., Shaw, J. H., Bottazzi, F., Caresani, F., Castineira, D., Cominelli, A., Mesa, M., Osculati, L., Petroselli, S., Plesch, A., (2021). A process-based approach to understanding and managing triggered seismicity. *Nature*, 595(7869), 684-689. https://doi.org/10.1038/s41586-021-03668-z
32. Jessell, M. W., Willman, C. E., & Gray, D. R. (1994). Bedding parallel veins and their relationship to folding. *Journal of Structural Geology*, *16*(6), 753-767. https://doi.org/10.1016/0191-8141(94)90143-0
33. Jiang, L., Cai, C., Worden, R. H., Li, K., Xiang, L., Chu, X., Shen, A. & Li, W. (2015). Rare earth element and yttrium (REY) geochemistry in carbonate reservoirs during deep burial diagenesis: Implications for REY mobility during thermochemical sulfate reduction. *Chemical Geology*, *415*, 87-101. https://doi.org/10.1016/j.chemgeo.2015.09.010
34. Jin, Z., Cao, J., Hu, W., Zhang, Y., Yao, S., Wang, X., Zhang, Y., Tang, Y., & Shi, X. (2008). Episodic petroleum fluid migration in fault zones of the northwestern Junggar Basin (northwest China): Evidence from hydrocarbon-bearing zoned calcite cement. *AAPG bulletin*, *92*(9), 1225-1243. https://doi.org/10.1306/06050807124
35. Iannace, A., Gasparrini, M., Gabellone, T., & Mazzoli, S. (2012). Late dolomitization in basinal limestones of the southern Apennines fold and thrust belt (Italy). *Oil & gas science and technology*, *67*(1), 59-75. https://dx.doi.org/10.2516/ogst/2011166
36. Improta, L., Bagh, S., De Gori, P., Valoroso, L., Pastori, M., Piccinini, D., Chiarabba, C., Anselmi, M., Buttinelli, M. (2017). Reservoir structure and wastewater-induced seismicity at the Val d'Agri Oilfield (Italy) shown by three-dimensional Vp and Vp/Vs local earthquake tomography. *Journal of Geophysical Research: Solid Earth*, 122(11), 9050-9082. https://doi.org/10.1002/2017JB014725
37. Italiano, F., Martelli, M., Martinelli, G., Nuccio, P. M., & Paternoster, M. (2001). Significance of earthquake-related anomalies in fluids of Val D’Agri (southern Italy). *Terra Nova*, *13*(4), 249-257. https://doi.org/10.1046/j.1365-3121.2001.00346.x

38. Malinverno, A., & Ryan, W. B., (1986). Extension in the Tyrrhenian Sea and shortening in the Apennines as result of arc migration driven by sinking of the lithosphere. *Tectonics*, 5(2), 227–245. https://doi.org/10.1029/TC005i002p00227
39. Maggi, C., Frepoli, A., Cimini, G. B., Console, R., Chiappini, M., (2009). Recent seismicity and crustal stress field in the Lucanian Apennines and surrounding areas (Southern Italy): Seismotectonic implications. *Tectonophysics*, 463(1-4), 130-144. https://doi.org/10.1016/j.tecto.2008.09.032
40. Mancini, M., D'Anastasio, E., Barbieri, M., & De Martini, P. M. (2007). Geomorphological, paleontological and 87Sr/86Sr isotope analyses of early Pleistocene paleoshorelines to define the uplift of Central Apennines (Italy). *Quaternary Research*, *67*(3), 487-501. doi:10.1016/j.yqres.2007.01.005
41. Manniello, C., Abdallah, I. B., Prosser, G., & Agosta, F. (2023). Pressure solution-assisted diagenesis and thrusting-related deformation of Mesozoic platform carbonates. *Journal of Structural Geology*, 104906. https://doi.org/10.1016/j.jsg.2023.104906
42. Mariucci, M. T., Montone, P., 2020. Database of Italian present-day stress indicators, IPSI 1.4. Scientific data, 7(1), 298. https://doi.org/10.1038/s41597-020-00640-w
43. Maschio, L., Ferranti, L., & Burrato, P., (2005). Active extension in Val d'Agri area, Southern Apennines, Italy: implications for the geometry of the seismogenic belt. *Geophysical Journal International*, 162(2), 591-609. https://doi.org/10.1111/j.1365-246X.2005.02597.x
44. Mazzoli, S., Barkham, S., Cello, G., Gambini, R., Mattioni, L., Shiner, P., Tondi, E., (2001). Reconstruction of continental margin architecture deformed by the contraction of the Lagonegro Basin, southern Apennines, Italy. *Journal of the Geological Society*, 158(2), 309-319. https://doi.org/10.1144/jgs.158.2.309
45. Mazzoli, S., Invernizzi, C., Marchegiani, L., Mattioni, L., & Cello, G. (2004). Brittle-ductile shear zone evolution and fault initiation in limestones, Monte Cugnone (Lucania), southern Apennines, Italy. *Geological Society, London, Special Publications*, *224*(1), 353-373. https://doi.org/10.1144/GSL.SP.2004.224.01.22
46. McArthur, J. M., Howarth, R. J., & Bailey, T. R. (2001). Strontium isotope stratigraphy: LOWESS version 3: best fit to the marine Sr-isotope curve for 0–509 Ma and accompanying look-up table for deriving numerical age. *The Journal of Geology*, *109*(2), 155-170. https://doi.org/10.1086/319243
47. McLennan, S.M. (1989) Rare Earth Elements in Sedimentary Rocks: Influence of Provenance and Sedimentary Processes. In: Lipin, B.R. and McKay, G.A., Eds., Geochemistry and Mineralogy of Rare Earth Elements, De Gruyter, Berlin, 169-200. https://doi.org/10.1515/9781501509032-010

48. Miller, S. A., Collettini, C., Chiaraluce, L., Cocco, M., Barchi, M., & Kaus, B. J. (2004). Aftershocks driven by a high-pressure CO2 source at depth. *Nature*, *427*(6976), 724-727. https://doi.org/10.1038/nature02251
49. Müller, I. A., Fernandez, A., Radke, J., Van Dijk, J., Bowen, D., Schwieters, J., & Bernasconi, S. M. (2017). Carbonate clumped isotope analyses with the long-integration dual-inlet (LIDI) workflow: Scratching at the lower sample weight boundaries. *Rapid Communications in Mass Spectrometry*, *31*(12), 1057-1066. https://doi.org/10.1002/rcm.7878
50. O'Neil, J. R., Clayton, R. N., & Mayeda, T. K. (1969). Oxygen isotope fractionation in divalent metal carbonates. The Journal of Chemical Physics, 51(12), 5547-5558. https://doi.org/10.1063/1.1671982
51. Palladino, G., Prosser, G., Olita, F., Avagliano, D., Dello Iacovo, B., Giano, S. I., Bentivenga, M., Agosta, F., & Grimaldi, S. (2023). Reconstruction of the structural setting of the north-eastern side of the high Agri Valley (Southern Apennines, Italy) based on detailed field mapping. Journal of Maps, 19(1), 2257729. https://doi.org/10.1080/17445647.2023.2257729
52. Patacca, E., Scandone, P., (2007). Geology of the southern Apennines. Bollettino della Società Geologica Italiana, 7, 75-119.
53. Roberts, N. M., & Holdsworth, R. E. (2022). Timescales of faulting through calcite geochronology: a review. *Journal of Structural Geology*, *158*, 104578. https://doi.org/10.1016/j.jsg.2022.104578
54. Schirripa Spagnolo, G., Agosta, F., Aldega, L., Prosser, G., Smeraglia, L., Tavani, S., Looser, N., Guillong, M., Bernasconi, S.M., Billi, A., & Carminati, E., (2024). Structural architecture and maturity of Val d'Agri faults, Italy: inferences from natural and induced seismicity. Journal of Structural Geology, 105084. https://doi.org/10.1016/j.jsg.2024.105084
55. Sharp, Z., (2017). Principles of Stable Isotope Geochemistry, 2nd Edition. https://doi.org/10.25844/h9q1-0p82
56. Shiner, P., Beccacini, A., Mazzoli, S., (2004). Thin-skinned versus thick-skinned structural models for Apulian carbonate reservoirs: constraints from the Val d'Agri Fields, S Apennines, Italy. *Marine and Petroleum Geology*, 21(7), 805-827. https://doi.org/10.1016/j.marpetgeo.2003.11.020
57. Shukla, R., Ranjith, P., Haque, A., & Choi, X. (2010). A review of studies on CO_2 sequestration and caprock integrity. *Fuel*, *89*(10), 2651-2664. https://doi.org/10.1016/j.fuel.2010.05.012
58. Sibson, R. H. (2000). Fluid involvement in normal faulting. *Journal of Geodynamics*, *29*(3-5), 469-499. https://doi.org/10.1016/S0264-3707(99)00042-3

59. Sibson, R. H. (2020). Preparation zones for large crustal earthquakes consequent on fault-valve action. *Earth, Planets and Space*, *72*, 1-20. https://doi.org/10.1186/s40623-020-01153-x

60. Smeraglia, L., Aldega, L., Bernasconi, S. M., Billi, A., Boschi, C., Caracausi, A., Carminati E., Franchini S., Rizzo A.L., Rossetti F., & Vignaroli, G. (2020). The role of trapped fluids during the development and deformation of a carbonate/shale intra-wedge tectonic mélange (Mt. Massico, Southern Apennines, Italy). *Journal of Structural Geology*, *138*, 104086. https://doi.org/10.1016/j.jsg.2020.104086

61. Song, X., Wang, H., Fu, X., Meng, L., Sun, Y., Liu, Z., & Du, R. (2022). Hydrocarbon retention and leakage in traps bounded by active faults: A case study from traps along the NDG fault in the Qinan area, Bohai Bay Basin, China. *Journal of Petroleum Science and Engineering*, *208*, 109344. https://doi.org/10.1016/j.petrol.2021.109344

62. Środoń, J. Nature of mixed layer clays and mechanisms of their formation and alteration (1999). Annu. Rev. Earth Pl. Sc. 27, 19-53. https://doi.org/10.1146/annurev.earth.27.1.19

63. Tostevin, R., Shields, G. A., Tarbuck, G. M., He, T., Clarkson, M. O., & Wood, R. A. (2016). Effective use of cerium anomalies as a redox proxy in carbonate-dominated marine settings. *Chemical Geology*, *438*, 146-162. https://doi.org/10.1016/j.chemgeo.2016.06.027

64. Uysal, I. T., Feng, Y. X., Zhao, J. X., Bolhar, R., Işik, V., Baublys, K. A., Yago, A., & Golding, S. D. (2011). Seismic cycles recorded in late Quaternary calcite veins: geochronological, geochemical and microstructural evidence. *Earth and Planetary Science Letters*, *303*(1-2), 84-96. doi:10.1016/j.epsl.2010.12.039

65. Valoroso, L., Piccinini, D., Improta, L., Gaviano, S., & Giunchi, C. (2023). Characterizing Seismogenic Fault Structures of the Lake Pertusillo Reservoir Induced Seismicity (Southern Italy) Using a Relocated Template-Matching Catalog. *Journal of Geophysical Research: Solid Earth*, *128*(7), e2022JB025879. https://doi.org/10.1029/2022JB025879

66. Van Der Pluijm, B.A. and Marshak, S. (2004) Earth Structure: An Introduction to Structural Geology and Tectonics. 2nd Edition, WW Norton, New York.

67. Vitale, S., & Ciarcia, S. (2018). Tectono-stratigraphic setting of the Campania region (southern Italy). *Journal of Maps*, *14*(2), 9-21. https://doi.org/10.1080/17445647.2018.1424655